of magnetic, librational, and vibrational levels. Inelastic features have indeed been observed in the range 3–50 meV, and these will be the subject of a future investigation.[10]

Returning to the fixed-window data, plots of ln $[S(Q,\omega \approx 0)]$ versus Q^2 give straight lines from which $\langle u^2 \rangle$ can be calculated (see eq 1). Typical plots are shown in Figure 3a. There is considerable scatter, because (1) each point represents only 4.75 min of data collection at the low neutron flux used and because (2) while corrections for detector efficiency have been applied, contributions from Bragg scattering have not been eliminated. What can be seen however is a clear difference in gradient, implying different amplitudes of proton motion, between the lowest (51 K) and the highest (287 K) temperatures. To confirm this, a second set of experiments was performed, scanning over a range of ω. Data in the range $(h/2\pi)\omega = -4$ to $+4$ μeV were extracted from these scans and taken as measures of $S(Q,0)$. Only four temperatures were used, but the measuring time was extended to 20 h in each case, and the detectors were regrouped, so that sets of four consecutive angles were summed together. With all these improvements in the statistics, plots of ln $[S(Q,0)]$ versus Q^2 gave much better straight lines, as shown in Figure 3b.

Values of $\langle u^2 \rangle^{1/2}$ obtained by these two methods are plotted against temperature in Figure 2c and can be seen to agree well. In the range 50–220 K, values go from 0.28 to 0.4 Å, and there is no break in the curve near 112 K, in contrast to the elastic scan data shown in Figure 2b. The gradient of the curve however increases over the range 230–287 K, with $\langle u^2 \rangle^{1/2}$ reaching about 0.5 Å at the upper end of the range. Contributions to $\langle u^2 \rangle^{1/2}$ come from all moving parts of the molecule, but they are dominated by the hydrogenous parts, i.e. the pyridine molecules. In the crystal structure[5] the coordinated pyridines are stacked parallel to each other, as shown in Figure 1, and their motions must be relatively restricted; hence the increase in $\langle u^2 \rangle^{1/2}$ must reflect mainly motions of the noncoordinated pyridines, which are held only by weak lattice forces. Within the statistics, the data are consistent with the onset of rotational motion at around $T = T_{c1} \approx 190$ K. Quasielastic scattering experiments are in progress to characterize this motion more precisely.

Conclusion

What is clear from the present work is that there are striking correspondences between the elastic scattering probability and other physical measurements, especially the specific heat data of Sorai et al. In particular, the first-order transition shown by the specific heat data coincides with a discontinuous change in the scattering probability, while the second-order transition coincides with a gradual change in the gradient of the scattering profile. The steepest gradient of the profile agrees with the region of maximum entropy gain of the sample.

Acknowledgment. We thank the Science and Engineering Research Council for the provision of beam time and the Kenya State Ministry of Education for a scholarship to S.K.a-K.

(10) Jayasooriya, U. A.; Cannon, R. D.; arapKoske, S. K.; Anson, C. E.; White, R. P.; Kearley, G. D. ILL Experimental Report 9-08-39 (January, 18, 1991); full manuscript in preparation.

Unprecedented and Reversible Cobalt-to-Carbon Alkyl Bond Rearrangement in the Coenzyme B_{12} Model Complex $C_6H_5CH_2Co^{III}[C_2(DO)(DOH)_{pn}]I$: Synthesis, Structural Characterization, and Mechanistic Studies

Brian E. Daikh[1] and Richard G. Finke*

Contribution from the Department of Chemistry, University of Oregon, Eugene, Oregon 97403. *Received October 26, 1990*

Abstract: Photolysis of the coenzyme B_{12} model complex $PhCH_2Co[C_2(DO)(DOH)_{pn}]I$ (**1**) leads to a high-yield, efficient synthesis of an unprecedented cobalt-to-carbon alkyl rearrangement product $Co[C_2(DO)(DOH)_{pn}CH_2Ph]I$ (**2**), (*SP*-5-15)-[2-[[3-[[2-(hydroxyamino)-1-methyl-2-(phenylmethyl)butylidene]amino]propyl]imino]-3-pentanone oximato(2-)-*N*,*N*′,*N*″,*N*‴]iodocobalt. The novel product **2** is unequivocally characterized by X-ray crystallography, ^{1}H NMR, visible, and mass spectroscopy, and an elemental analysis. With pure **2** available, a thermal equilibrium between **1** and **2**, $K_{eq} = 1.5 \pm 0.1$ (69 °C, benzene solvent), is shown to exist, thereby explaining the low (60%) yield of **2** from the thermolysis of **1** at 69 °C. Thermolysis of **2** in the presence of TEMPO free radical trap quantitatively yields trapped benzylTEMPO and $^{\bullet}Co^{II}[C_2(DO)(DOH)_{pn}]I$. An Eyring plot of this reaction yields $\Delta H^{\ddagger} = 26 \pm 2$ kcal/mol, $\Delta S^{\ddagger} = -6 \pm 7$ cal/(mol·K), or $\Delta G^{\ddagger}_{298} = 27 \pm 3$ kcal/mol; the $\Delta H^{\ddagger}$ value plus appropriate corrections imply a low benzyl–carbon bond dissociation energy of 25 kcal/mol in **2**. Also provided are a proposed mechanism for the formation of **2**, a summary discussion detailing the significance of the results toward explaining a number of related, but poorly understood, literature reports, and a short list of some interesting but unanswered questions that form a basis for future research.

Previously,[2] in developing the now widely used[3-5] nitroxide radical trapping method for studying cobalt–carbon[3,4] and other metal–carbon[3,5] bond homolyses, we examined the thermolysis of the orange-brown benzyl coenzyme B_{12} model complex

(1) (a) Undergraduate research associate and University of Oregon Honors College Thesis Student. (b) Daikh, B. E., Synthesis Characterization, and Kinetic and Mechanistic Studies of an Unusual Cobalt-to-Carbon Bond Alkyl Rearrangement in the Coenzyme B_{12} Model Complex $C_6H_5CH_2Co^{(III)}[(DO)(DOH)_{pn}]I$. University of Oregon Honors College Thesis, Eugene, OR, May 9, 1990.

(2) (a) Finke, R. G.; Smith, B. L.; Mayer, B. J.; Molinero, A. A. *Inorg. Chem.* **1983**, *22*, 3677. (b) Smith, B. L. Ph.D. Dissertation, University of Oregon, Eugene, OR, 1982. (c) Aromatic solvents were used[2a,b] since formation of $PhCH_3$ by H$^{\bullet}$ abstraction from the solvent cannot[2a,b] occur given thermochemical ($PhCH_2$–H versus Ph–H bond energy) considerations.

0002-7863/91/1513-4160$02.50/0

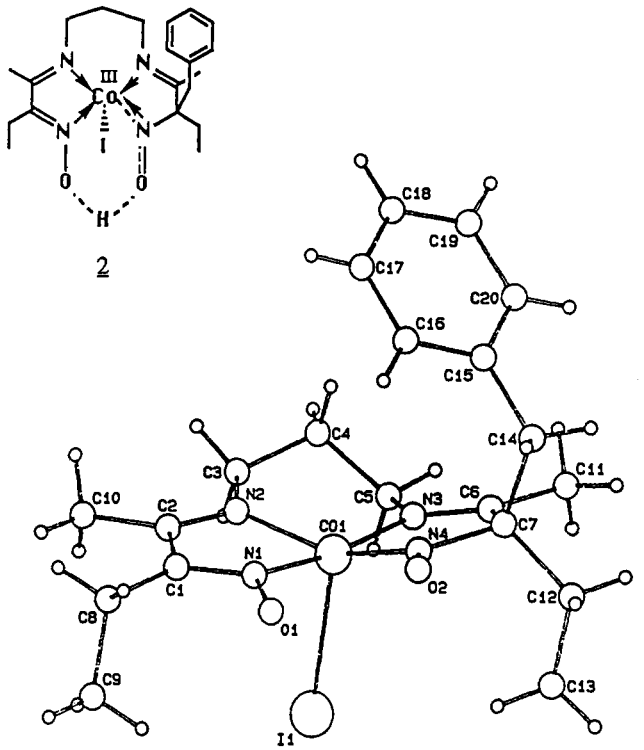

Figure 1. X-ray crystallographically determined molecular structure of the cobalt-to-carbon alkyl migration product **2**, (*SP*-5-15)-[2-[[3-[[2-(hydroxyamino)-1-methyl-2-(phenylmethyl)butylidene]amino]propyl]imino]-3-pentanone oximato(2−)-*N,N′,N″,N‴*]iodocobalt. The dashed lines between Co–N and N–O atoms in the inset structure indicate increased (probably double) bonding between those pairs of atoms, while the dashed O--H--O lines indicate the presence of two tautomers (see the text).

$C_6H_5CH_2Co^{III}[C_2(DO)(DOH)_{pn}]I$[6] (**1**) both with[2a] and without[2b,7a] the nitroxide TEMPO (eq 1). Unexpectedly, in the absence of

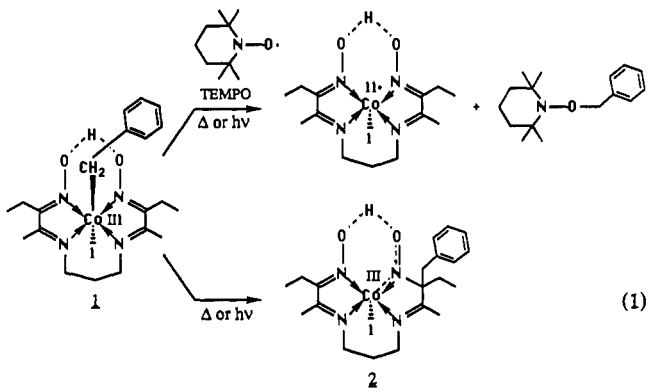

(1)

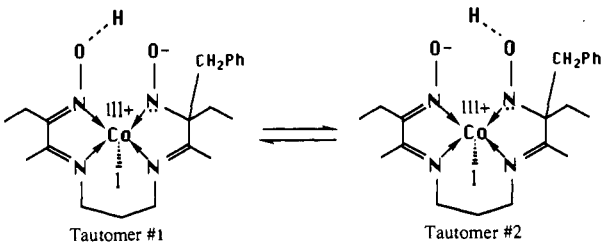

Figure 2. Two proposed tautomers of **2**.

TEMPO none of the expected bibenzyl product[2a,7c] was formed (<5% by NMR).[2c] Instead, a curious blood-red product, **2** (λ_{max} = 525 nm), is produced that initially appeared to be similar to paramagnetic, red $^{\bullet}Co^{II}[C_2(DO)(DOH)_{pn}]I$.[6a] However, ^1H NMR (vide infra) indicates that **2** is in fact diamagnetic *and still contains the benzyl group in what is a low* (C_1) *symmetry structural isomer of* **1**. Subsequent work, reported in a preliminary communication,[7a] demonstrated that the blood-red product is the result of the rearrangement of **1** to **2**.

Herein we report the full details of the clean, high-yield photochemical synthesis of **2**, its definitive characterization (by X-ray crystallography)[7a] as the novel cobalt-to-carbon (*not* the purported cobalt-to-nitrogen)[8] alkyl rearrangement product[9] (Figure 1), demonstration that the rearrangement of **1** to **2** is *reversible*, quantitation of the equilibrium constant for the thermal rearrangement **1** ⇌ **2**, and kinetic and mechanistic studies of the reverse reaction of **2** to **1**, including evidence for a low benzyl–carbon bond-dissociation energy (BDE) of 25 kcal/mol in **2**.[7b]

In addition to the above findings, the further significance of this work is its relationship to a growing body of literature, specifically: (1) The unequivocal structural characterization of **2** provides the first firm precedent from which to reinterpret scattered reports since 1975 of generally ill-characterized and thus

(3) (a) The nitroxide method has subsequently proven to be the method of choice for B_{12} alkyls[3b-d] [including coenzyme B_{12},[4a,b] AdoCbi$^+$ (base-free B_{12}),[4c] MeB_{12},[4d] and neopentyl B_{12}[4e]] as well as non-B_{12} systems.[5] (b) Bakac, A.; Espenson, J. H. *J. Am. Chem. Soc.* **1984**, *106*, 5197. Blau, R. J.; Espenson, J. H. *J. Am. Chem. Soc.* **1985**, *107*, 3530. (c) Geno, M. K.; Halpern, J. *J. Am. Chem. Soc.* **1987**, *109*, 1238. Geno, M. K.; Halpern, J. *J. Chem. Soc., Chem. Commun.* **1987**, 1052. (d) Gamelkoorn, H. J.; de Bolster, M. W. G.; Bait, S., private communication of unpublished results.

(4) (a) For Coenzyme B_{12}'s thermolysis and associated BDE, see: Finke, R. G.; Hay, B. P. *Inorg. Chem.* **1984**, *23*, 3041. (b) Full paper: Hay, B. P.; Finke, R. G. *Polyhedron* **1988**, *7*, 1469. (c) AdoCbi$^+$ thermolysis and BDE: Hay, B. P.; Finke, R. G. *J. Am. Chem. Soc.* **1987**, *109*, 8012. (d) MeB_{12} thermolysis and BDE: Martin, B. D.; Finke, R. G. *J. Am. Chem. Soc.* **1990**, *112*, 2419. (e) Neopentyl B_{12} thermolysis and BDE: Waddington, M.; Finke, R. G., submitted for publication.

(5) Collman, J. P.; McElwee-White, L.; Brothers, P. J.; Rose, E. *J. Am. Chem. Soc.* **1986**, *108*, 1332.

(6) (a) Finke, R. G.; Smith, B. L.; McKenna, W. A.; Christian, P. A. *Inorg. Chem.* **1981**, *20*, 687. (b) The $Co[C_2(DO)(DOH)_{pn}]$ or equivalently[6c,d] Co[EMO(EMOH)] "modified-Costa"[6a] B_{12} model is shown in eq 1. The $C_2(DO)(DOH)_{pn}$ ligand therein is 2,10-diethyl-3,9-dimethyl-1,4,8,11-tetraazaundeca-1,3,8,10-tetraene-1,11-diol. The IUPAC nomenclature for **2** is given in the caption for Figure 1. (c) Marzilli, L.; Bresciani-Pahor, N.; Randaccio, L.; Zangrando, E.; Finke, R.; Myers, S. *Inorg. Chim. Acta* **1985**, *107*, 139. (d) Parker, W.; Bresciani-Pahor, N.; Zangrando, E.; Randaccio, L.; Marzilli, L. *Inorg. Chem.* **1985**, *24*, 3908; *Inorg. Chem.* **1986**, *25*, 1303; *Inorg. Chem.* **1986**, *25*, 3489; *Gazz. Chim. Ital.* **1987**, *117*, 307.

(7) (a) Daikh, B. E.; Hutchison, J. E.; Gray, N. E.; Smith, B. L.; Weakley, T. J. R.; Finke, R. G. *J. Am. Chem. Soc.* **1990**, *112*, 7830. (b) Daikh, B. E.; Finke, R. G. *J. Chem. Soc., Chem. Commun.*, in press. (c) Quantitation of the exact amount of bibenzyl and further kinetic modeling are under separate investigation (experiments in progress).

(8) Anaerobic photolysis of cobaloxime and related B_{12} models is purported to yield ligand–N–R products, despite their inadequate characterization or quantitation, see: (a) Gianotti, C.; Merle, G.; Fontaine, C. *J. Organomet. Chem.* **1975**, *91*, 357. (b) Gianotti, C.; Merle, G.; Bolton, J. R. *J. Organomet. Chem.* **1975**, *99*, 145. (c) Gianotti, C.; Bolton, J. R. *J. Organomet. Chem.* **1976**, *110*, 383. (d) Maillard, P.; Massot, J. C.; Gianotti, C. *J. Organomet. Chem.* **1978**, *159*, 219. (e) LeHoang, M. D.; Robin, Y.; Devynck, J.; Bied-Charreton, C.; Gaudemer, A. *J. Organomet. Chem.* **1981**, *222*, 311.

(9) Several interesting and thorough studies of possibly related reactions are available, but these generally involve unstable intermediates whose unequivocal structural characterization has also not proven possible. (a) C–R or N–R intermediates are acknowledged, but the latter are favored, in the reactions of R-cobaloximes with R′• free radicals: McHatton, R.; Espenson, J.; Bakac, A. *J. Am. Chem. Soc.* **1986**, *108*, 5885. Note that R′ = benzyl does not yield an RCH_2Ph product in this study. (b) A SALEN ligand N–R intermediate is proposed in: Samsel, E. G.; Kochi, J. K. *J. Am. Chem. Soc.* **1986**, *106*, 4790. (c) Following $IrCl_6^{2-}$ oxidation, benzylcobaloxime produces a NCH_2Ph (or possibly $NOCH_2Ph$) containing ligand fragment by NMR and mass spectroscopy: Abley, P.; Dockal, E.; Halpern, J. *J. Am. Chem. Soc.* **1972**, *94*, 659. This same product is also formed when benzylcobaloxime reacts with $Mn(OAc)_3$: Gaudemer, F.; Gaudemer, A. *Tetrahedron Lett.* **1980**, *21*, 1445. (d) Ligand-O-R intermediates are proposed following electrochemical oxidation of RCo(SALEN) and RCo(SALPHEN) complexes: Vol'pin, M. E.; Levitin, I. Y.; Sigan, A. L.; Halpern, J.; Tom, G. M. *Inorg. Chim. Acta* **1980**, *41*, 271. (e) Electrochemical reduction of a neopentyl B_{12} Costa-type model yields a Co^{II} species; it is proposed that "the neopentyl group may have migrated onto the equatorial ligand in the reduced species"; see: Seeber, R.; Marassi, R.; Parker, W. O., Jr.; Marzilli, L. G. *Organometallics* **1988**, *7*, 1672.

uncertain anaerobic photolysis or thermolysis products in B_{12} model systems.[8] In several cases a reexamination of the literature[8,9a,b] is probably warranted. (2) The present report extends the growing body of such alkyl migrations to metal–macrocycle ring systems other than metalloporphyrins.[10] (3) Our work also suggests, especially when combined with the burgeoning literature employing alkylcobaloximes as alkyl radical precursors in organic synthesis,[11] the existence of similar—but as of yet uncharacterized—products[11b] related to that organic synthesis literature.[8] (4) The results presented herein provide precedent for cobalt-to-carbon alkyl migrations as possible catalyst and stoichiometric reagent deactivation pathways. And perhaps most importantly, (5) the present work raises the question of the possible existence,[12] and, if so, the implications, of analogous chemistry in B_{12} itself. The latter question is presently under separate investigation.[13]

Results

Synthesis and Characterization. Synthesis of 2. Analytically pure **2** is synthesized photochemically (but not thermochemically, vide infra) from **1**, at both high and low starting concentrations of **1**, in excellent yield (100 ± 5% by NMR and visible spectroscopy[14]) and in sufficient quantity (47–125 mg). The photolysis of **1** is complete within about 20 min by visible spectroscopy under the conditions detailed under Experimental Section. The reaction is conveniently monitored by the absorbance decrease with time of the λ_{max} of **1** at 417 nm or by the absorbance increase of the λ_{max} of **2** at 525 nm; an isosbestic at 466 nm is maintained throughout this conversion. ^{1}H NMR data confirm that the photolytic formation of **2** from **1** is clean (i.e., there are no other NMR-detectable products or intermediates formed). Although some of the rearrangement product **2** is also produced from the thermolysis of **1**, this reaction is not quantitative, but instead yields an *equilibrium mixture* of **1** and **2** in a 40 ± 2%:60 ± 2% ratio, respectively; K_{eq} = 1.5 ± 0.1. This result is discussed in greater detail in the section below titled Equilibrium Studies as a Function of Temperature.

X-ray Crystal Structure of 2. The crystallographic analysis[7a] reveals (Figure 1) an unprecedented *cobalt-to-carbon* migration of the benzyl group as **1** is converted to **2** (not the widely proposed but unsubstantiated migration to nitrogen).[8,9] The benzyl group has migrated from the sixth coordination site on Co(1), trans to I(1), to the atom C(7) adjacent to the oxime nitrogen atom N(4). It remains on the side of the ring system remote from I(1). The ring system itself in Figure 1 can be considered in three parts.

(1) The chelate ring Co(1)–N(1)–C(1)–C(2)–N(2) is planar to within 0.08 Å. The Co(1)–N(1) (oxime) and Co(1)–N(2) (imine) bond lengths are respectively at the lower and upper limits of the ranges observed in related complexes.[6c,d,15] Other di-

Table I. Crystallographic Data

formula	$C_{20}H_{30}CoIN_4O_2 \cdot 0.5C_6H_6$
system, space group	triclinic, $P\bar{1}$
a, b, c, Å	9.966 (1), 16.514 (3), 7.892 (3)
α, β, ρ	101.42 (2), 90.66 (2), 77.70 (1)
V, Å^3	1243 (1)
Z	2
D_{calc}, g cm^{-3}	1.56
μ, cm^{-1}	20.0
F_{000}	594
intensity measurement	
cryst appearance	black lath
cryst size, mm	0.30 × 0.15 × 0.07
diffractometer	Rigaku AFC6R
radiation, λ, Å	Mo Kα, 0.710 69
monochromator	graphite
transmissn factors	0.84–1.00
absorptn correctn	ψ-scan
scan mode	ω–2θ
scan width, deg	0.84 + 0.30 tan θ
scan speed, ω, deg min^{-1}	16
$2\theta_{max}$	50.2
octants	$+h,\pm k,\pm l$
T, °C	23
no. of reflcns scanned (total)	4702
no. of reflcns (independent)	4422
std reflcns	3, every 150 (no change)
R_{int}, $\pm(0kl)$	0.010
refinement (on F):	
no. of obsd data	2258 [$I \geq 3\sigma(I)$]
no. of params	265
functn minimized	$\sum w(\lvert F_o\rvert - \lvert F_c\rvert)^2$
weighting factor	$\sigma^{-2}(F)$
R, wR	0.052, 0.061
goodness-of-fit index	1.29
max Δ/σ, last cycle	0.03

(10) Lead references to the extensive literature of metalloporphyrin (including iron, ruthenium, nickel, and cobalt porphyrins) alkyl-migration reactions: (a) *Cytochrome P-450: Structure, Mechanism, and Biochemistry*; Ortiz de Montellano, P. R., Ed.; Plenum Press: New York, 1986; Chapter 8 and references therein. (b) Lavalle, D. K. *The Chemistry and Biochemistry of N-Substituted Porphyrins*; VCH Publishers: New York, 1987; Chapter 7 and references therein. (c) De Matteis, F.; Cantoni, L. *Biochemistry* **1979**, *183*, 99. (d) Mansuy, D. *Pure Appl. Chem.* **1987**, *59*, 759; **1980**, *52*, 681. (e) Artaud, I.; Devocelle, L.; Battioni, J.-P.; Girault, J.-P.; Mansuy, D. *J. Am. Chem. Soc.* **1987**, *109*, 3782. (f) Artaud, I.; Gregoire, N.; Battioni, J.-P.; Dupre, D.; Mansuy, D. *J. Am. Chem. Soc.* **1988**, *110*, 8714 and references therein. (g) Callot, H. J.; Schaffer, E. *Tetrahedron Lett.* **1980**, *21*, 1335. (h) Callot, H. J.; Metz, F. *J. Chem. Soc., Chem. Commun.* **1982**, 947. (i) Dolphin, D.; Halko, D. J.; Johnson, E. *Inorg. Chem.* **1981**, *20*, 4348. (j) Mashiko, T.; Dolphin, D.; Nakamo, T.; Traylor, T. G. *J. Am. Chem. Soc.* **1985**, *107*, 3735. (k) Traylor, T.; Mikszta, A. R. *J. Am. Chem. Soc.* **1987**, *109*, 2770. (l) Chevrier, B.; Weiss, R. *J. Am. Chem. Soc.* **1981**, *103*, 2899; *J. Am. Chem. Soc.* **1976**, *98*, 2985. (m) Latos-Grazynski, L.; Cheng, R. J.; La Mar, G.; Balch, A. *J. Am. Chem. Soc.* **1981**, *103*, 4270. (n) Lancon, D.; Cocollos, P.; Guilard, R.; Kadish, K. M. *J. Am. Chem. Soc.* **1984**, *106*, 4472; *Organometallics* **1984**, *3*, 1164. (o) Castro, C. E.; Wade, R. S. *J. Org. Chem.* **1985**, *50*, 5342. (p) Collman, J. P.; Hampton, P. D.; Brauman, J. I. *J. Am. Chem. Soc.* **1990**, *112*, 2977 and references therein; **1990**, *112*, 2986. (q) Ortiz de Montellano, P. R.; Kunze, K. L.; Augusto, O. *J. Am. Chem. Soc.* **1982**, *104*, 3545. (r) Ortis de Montellano, P. R.; Kunze, K. L. *J. Am. Chem. Soc.* **1981**, *103*, 6534. (s) Wisnieff, T. J.; Gold, A.; Evans, S. A., Jr. *J. Am. Chem. Soc.* **1981**, *103*, 5616. (t) Chan, Y. W.; Wood, F. E.; Renner, M. W.; Hope, H.; Balch, A. L. *J. Am. Chem. Soc.* **1984**, *106*, 3380.

(11) Lead references: (a) Tada, M.; Okabe, M. *Chem. Lett.* **1980**, 201. Okabe, M.; Tada, M. *Chem. Lett.* **1980**, 831. (b) Branchaud, B. P.; Meier, M. S.; Malekzadeh, M. N. *J. Org. Chem.* **1987**, *52*, 212 and references therein. Note that these authors report (p 216) 14–26% of uncharacterized products, "presumably derived from the ligand", are formed that adhere to silica gel as dark-colored material. (c) Bandaranayake, W. M.; Pattenden, G. *J. Chem. Soc., Chem. Commun.* **1988**, 1179 and earlier references in this series. (d) Baldwin, J.; Li, C. S. *J. Chem. Soc., Chem. Commun.* **1988**, 261; **1987**, 166.

(12) (a) An interesting report (among others)[12b-d] in this regard is one describing the "incipient homolysis" of coenzyme B_{12} following photolysis in a frozen H_2O/propylene glycol matrix at −193 to −73 °C: Lowe, D. J.; Joblin, K. N.; Cardin, D. J. *Biochim. Biophys. Acta* **1978**, *539*, 398. (b) Ramakrishna Rao, D. N.; Symons, M. C. R. *J. Chem. Soc., Chem. Commun.* **1982**, 954. (c) Ramakrishna Rao, D. N.; Symons, M. C. R. *J. Chem. Soc., Perkin Trans. II* **1983**, 187. (d) See also ref 3.

(13) Daikh, B. E.; Finke, R. G. Experiments in progress. *Note Added In Proof*: Our reinvestigation of some aspects of Hogenkamp's work[33] indicates that no methyl-to-corrin migration products are seen in the anaerobic photolysis of MeB_{12}. Methylcobalamin (>98% pure) was dissolved in strictly anaerobic (5× frozen–pumped–thawed) unbuffered aqueous solution (0.02M) and then photolysed in a quartz cuvette 15 cm from a 475-W immersion lamp until there was no change the UV/visible spectra (obtained by diluting the reaction solution). The only corrin product detectable is Co^{II} B_{12r} (by UV/visible spectroscopy, ESR, and FAB-mass spectroscopy in comparison in each case to authentic, isolated B_{12r}). Hence, O_2 is required for the products seen by Hogenkamp and co-workers as their earliest work indicates;[33] intermediates such as $MeOOB_{12}$ seem probable given literature precedent[13b-e] and these are under further investigation. This is further evidence that the chemistry reported herein may be specific to compounds with nitrone-like functionality (see text and Scheme II) as in **1**. (b) Jensen, F. R.; Kishis, R. C. *J. Am. Chem. Soc.* **1975**, *97*, 5825 and references therein. (c) Giannotti, C.; Fontaine, G.; Chiaroni, A.; Richie, C. *J. Organomet. Chem.* **1976**, *113*, 57 and references therein. (d) Deniau, J.; Gaudemer, A. *J. Organomet. Chem.* **1980**, *191*, C1–C2. (e) Kendrick, M. J.; Al-Akhdar, W. *Inorg. Chem.* **1987**, *26*, 3972.

(14) Initially, experiments at low concentrations of **1** indicated the reaction did not proceed with a clean isosbestic point and showed that the final spectrum was not that of **2**. However, subsequent work revealed that this result is due to trace oxygen contamination since the rigorous air-free handling of the sample does yield the desired product quantitatively with a clean isosbestic point at 466 nm even at 10^{-4} M **1**. Any studies that reinvestigate earlier work[8,9] will want to note this result.

(15) Calligaris, M. *J. Chem. Soc. (London), Dalton Trans.* **1974**, 1628.

mensions are normal.

(2) The six-membered ring Co(1)–N(2)–C(3)–C(4)–C(5)–N-(3) is puckered, as expected. It shows no disorder as the central methylene atom C(4) occupies a single site on the side of the mean plane of the other five ring atoms remote from I(1).

(3) The ring Co(1)–N(3)–C(6)–C(7)–N(4) is planar to within 0.035 Å but its mean plane is inclined at 21° to the mean plane of the other five-membered ring. Interestingly, the change in bond hybridization at C(7) from sp^2 to sp^3, accompanying the benzyl group migration, has allowed N(3) to remain almost coplanar with Co(1), N(1), and N(2) but has displaced N(4) 0.69 Å above the Co(1), N(1,2,3) mean plane. Also both the N(4)–Co(1) and the N(4)–O(2) bond lengths [1.78 (1), 1.28 (1) Å] are significantly shorter than their "normal" counterparts N(1)–Co(1) and N-(1)–O(1) [1.86, 1.38 (1) Å], *indicating the increased bond order between these pairs of atoms.*

The O(1)···O(2) distance, 2.47 (1) Å, is at the upper end of the range of values found in related Co complexes.[6c,d,15] The hydrogen atom of the intramolecular –O··H··O– hydrogen bond could not be located crystallographically. The Co–I bond distance, 2.69 (7) Å, is outside of the range of values for non-alkyl axial ligands found in related Co complexes (2.045–2.121 Å).[6c,d,15] This increased bond length helps explain the enhanced I^- dissociation in **2** relative to that in $ICo^{III}[C_2(DO)(DOH)_{pn}]I$.[17] The phenyl ring is placed so as to hinder access to the vacant coordination site on Co(1), thereby giving rise to distinctive chemical shifts for the phenyl aromatic protons (vide infra), but the shortest C(phenyl)–Co distance [C (16), 3.79 (2) Å] is far too long for significant bonding. There are no short intermolecular contacts. (See Table I).

Beyond establishing the cobalt-to-carbon migration of the benzyl group, the next most interesting aspect of the structure is what this alkyl migration has done to the Co(1)–N(4) and N(4)–O(2) bonds. As noted above, both their bond distances have shortened in the conversion of **1** to **2**. For the Co(1)–N(4) bond, this suggests that there is an increase in N-σ donor character (and thus greater Co^{II}• character) but also a synergistic increase in π back-bonding. For the N(4)–O(2) bond, an increase in N=O double bond character is indicated.

Subsequent NMR [COSY and ATP (attached proton test)] experiments confirm that the major features found in the solid-state structure are maintained in solution. The NMR studies do, however, reveal one new and interesting piece of structural information regarding the –O··H··O– bridge in **2**. A small peak

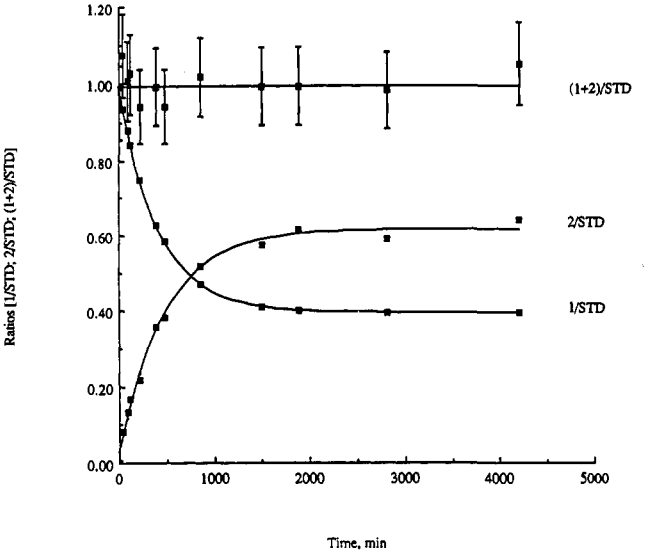

Figure 3. Plot of **1**/STD, **2**/STD, and (**1** + **2**)/STD for the integral data from the 69 °C thermolysis of **1** (STD equals Ph_3CH internal standard).

appears in the ^1H NMR spectrum of **2** at δ 17.37, just 0.1 ppm adjacent to the primary peak for the bridging hydroxylic proton at δ 17.47. Integration of the two peaks consistently yields a ratio of 9 ± 2%:91 ± 2%, respectively, even for different preparations or samples. Our immediate concern was whether or not we had crystallized the minor, 9% form of **2**. In a control experiment designed to test whether or not the crystalline form of **2** was the predominant (91%) or minor (9%) structural form, 500-MHz proton NMR of *single crystals* of **2** dissolved in benzene-d_6 revealed the *same two peaks in this same ratio.* The implied conclusion is that there are two distinct isomers of **2** in solution. Following a consideration of possible explanations[16] and their comparison to all of our data,[17,18] we conclude that the peaks at δ 17.37 and 17.47 reflect two different tautomers of **2** (Figure 2), that is, structural isomers differing only in the position of the bridging hydrogen.

Inspection of the structure, **2**, reveals that there are two accessible positions for the bridging hydroxylic proton to occupy in solution, either closer to O(1) or closer to O(2), as expected since **2** (C_1 symmetry) contains no mirror plane (e.g., as found in **1**). One of these must be more stable than the other (they cannot have *identical* stabilities except accidentally as they are chemically nonequivalent), hence the 91/9 ratio. Then, in the solid, crystalline phase, apparently either these two slightly different species co-crystallize with otherwise largely indistinguishable bond distances or, perhaps more likely, only one of the positions is preferred in the solid state. (Recall that the bridging hydroxylic proton could not be located in the crystal structure analysis.)

The conclusion that the two peaks are due to tautomers leads to experimental tests to support or refute this conclusion: the ratio of the two ^1H NMR peaks should be solvent dependent. Specifically, it should be different in nonprotic, nonpolar benzene (the solvent used above) than in polar nonprotic solvents (e.g., acetone) and also different in polar protic solvents (e.g., methanol). In fact, only in benzene are the two peaks seen. In all other solvents tested, only one peak is seen in the ^1H NMR.[17] Furthermore, variable-temperature ^1H NMR of **2** in benzene supports a tautomer explanation. At lower temperatures (7.5–20 °C), two distinct peaks are seen in the 91:9 ratio. However, as the temperature is increased from 30 to 70 °C and then returned to its original 30 °C value, the two peaks *reversibly* coalesce into a single peak and then back to the two original peaks. Thus, it appears that there are two positions (unequal in energy) for the bridging hydrogen to occupy and the exchange between these positions is slow relative to the NMR timescale at room or lower temperatures.[16,17]

(16) (a) A priori there appear to be five plausible explanations for the two downfield peaks in the ^1H NMR of **2**. (1) There could be two different solution structures of **2** differing only in the position of the bridging hydrogen (i.e., tautomers). (2) There could be two iodide-position structural isomers of **2** (each as a set of two enantiomers), one with the $PhCH_2$ group cis to the I atom, the other with the $PhCH_2$ group trans to the I atom. [The cis arrangement is inconsistent with the trans $PhCH_2$ and I found by X-ray crystallography (both trans enantiomers are found in the centrosymmetric space group; Figure A, supplementary material); the *possibility* of I^- dissociation once pure *trans*-**2** is dissolved is made very unlikely by the (non) conductivity experiments cited in the text.] (3) The I^- ion could dissociate a fraction (i.e., 9%) of the time, as this has some (minimal)[18] precedent. However, the conductivity experiments rule out this possibility as well. (4) The bridging hydrogen could be intramolecularly hydrogen-bonded to the phenyl ring of the benzyl group.[16b] (5) There could be some combination of the above possibilities. Given the results cited in the text, only the tautomer explanation is consistent with all the data. (b) Cotton, A. F.; Wilkinson, G. *Advanced Inorganic Chemistry: A Comprehensive Text*, 3rd ed.; Interscience Publishers: New York, 1972; Chapter 5, p 156, and ref 7 therein.

(17) (a) A careful search of the 500-MHz NMR revealed none of the expected splitting of the other peaks if in fact diastereomers of **2** were present or if the I^- was dissociating. In fact, no such peak splitting was detected. (See the Experimental Section "Experiments Designed to Test Tautomerization versus Other Conceivable Explanations..." for further details.) (b) The observation that the two peaks in the downfield ^1H NMR of **2** (at δ 17.47 and 17.37) are seen only in benzene implies that the observed proton shifts *in benzene* are due to *intramolecular* interactions (i.e., tautomerization), whereas in polar, and especially protic, solvents, *intermolecular* interactions with the solvent are dominant, resulting in only one downfield ^1H NMR peak. (c) Generally a single –O··H··O– peak is seen in the ^1H NMR, but intermolecular exchange of the bridging proton in cobaloximes occurs with a rate constant of ca. 50 s^{-1} at 25 °C. Dodd, D.; Johnson, M. D. *Organomet. Chem.* **1973**, *52*, 1.

(18) For conductivity experiments demonstrating I^- dissociation in CH_3CN from $ICo^{III}[C_2(DO)(DOH)_{pn}]I$, see: Finke, R. G.; McKenna, W. P.; Schiraldi, D. A.; Smith, B. L.; Pierpoint, C. *J. Am. Chem. Soc.* **1983**, *105*, 7592.

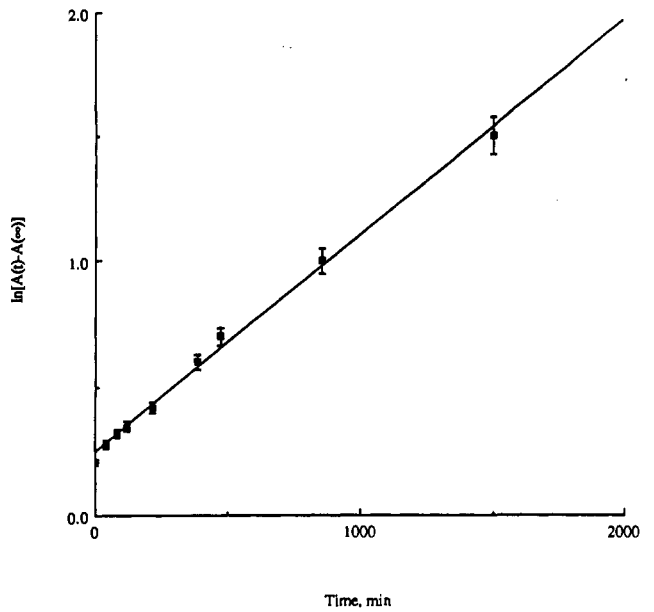

Figure 4. First-order plot of the ^1H NMR data from the 69 °C thermolysis of **1** to an equilibrium mixture of **1** and **2**.

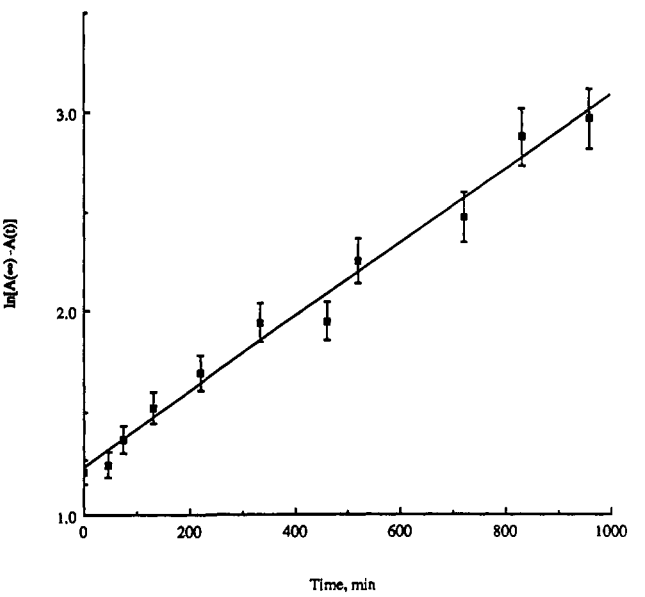

Figure 5. First-order plot of the ^1H NMR data from the 69 °C thermolysis of **2** to an equilibrium mixture of **1** and **2**.

Thermolysis Equilibrium Studies as a Function of Temperature. The 69 °C thermolysis of **1** at 1.5×10^{-2} M was complete within about 30 h by NMR. With the exception of the peaks corresponding to triphenylmethane (TPM) internal standard, all upfield proton peaks corresponded exactly and only to known peaks in the superimposed spectra of authentic **1** and **2**. Using the NMR integrals, the area of each downfield proton peak was normalized by dividing by the area of the TPM internal standard. The fraction of **1** was calculated [**1**/(**1** + **2**)] for each spectrum. The final equilibrium mixture was 40 ± 2% **1** and 60 ± 2% **2** (see Table II for a tabulation of the results of four experiments). These values yield $K_{eq} = 1.5 \pm 0.1$ and confirm why the thermolysis of **1** fails to yield 100% of **2**—an equilibrium-limited concentration of **2** is reached. The two fractions, **1**/TPM standard and **2**/TPM standard, were plotted versus time and gave very symmetrical curves (Figure 3). On the same plot, the sum of these two fractions was plotted versus time as well, demonstrating, as should be the case, that the sum of the two fractions remains constant and accounts for 100% of the material within experimental error (5%). These data suggest that *within the 5% limit of QE-300 NMR detection*, no other products (<5%) such as bibenzyl or $^{\bullet}Co^{II}[C_2(DO)(DOH)_{pn}]I$ are formed during the thermolysis of **1**.

Moreover, a visible spectrum of the equilibrium mixture of **1** and **2** matched very closely a mathematically weighted spectrum of 40% authentic **1** plus 60% authentic **2**. Upon photolysis of this equilibrium mixture, only peaks corresponding to **2** and TPM internal standard were visible by NMR, confirming that **2** is formed quantitatively from **1** by photolysis (and demonstrating the photochemical stability of the product **2**). The visible spectrum of this photolysis product confirmed the NMR by showing only the characteristic spectrum of **2** (λ_{max} at 525 nm).

Higher temperature (85 °C) thermolysis of **1** at 1.5×10^{-2} M was followed by NMR and gave the same equilibrium mixture within 2%. However, a precipitate was present and the resolution of the NMR was poor, likely due to the presence of the precipitate or $^{\bullet}Co^{II}[C_2(DO)(DOH)_{pn}]I$ formation or both. Clearly, some decomposition had occurred at this temperature and hence no further equilibrium experiments were conducted at 85 °C or higher temperatures.

Calculation of the equilibrium constant for the conversion of **1** to **2** at 69 °C gives $K_{eq69°} = 1.5 \pm 0.1$, which corresponds to a $\Delta G_{69°C} = -0.28 \pm 0.02$ kcal/mol. This result explains the previous puzzling question of the origin of the driving force for **1** → **2**; there is, overall, *relatively little driving force in this* $\Delta G \simeq 0$, $K_{eq} \simeq 1$ *reaction*. The essentially identical 69 and 85 °C K_{eq} values imply a near temperature-independent equilibrium, $\Delta H \simeq 0.00 \pm 0.02$ kcal/mol, from which $\Delta S = 0.82 \pm 0.06$ cal/(mol·K) can be calculated. Apparently, the thermolysis reaction is largely entropically driven.

Table II. 69 °C Thermolysis of **1** or **2** to Equilibrium

starting material	infinity point, % of **1** at equilib	k_{obs} ($k_{1,appl} + k_{-1,appl}$), s^{-1}
1	42	3.4×10^{-5}
1	41	3.0×10^{-5}
1	39	3.7×10^{-5}
2	39	3.3×10^{-5}
mean	40 ± 2	$(3.4 \pm 0.3) \times 10^{-5}$

Scheme I. Thermolysis of Either **1** or **2** Individually with (lower products) and without (upper equilibrium) TEMPO Free Radical Trap

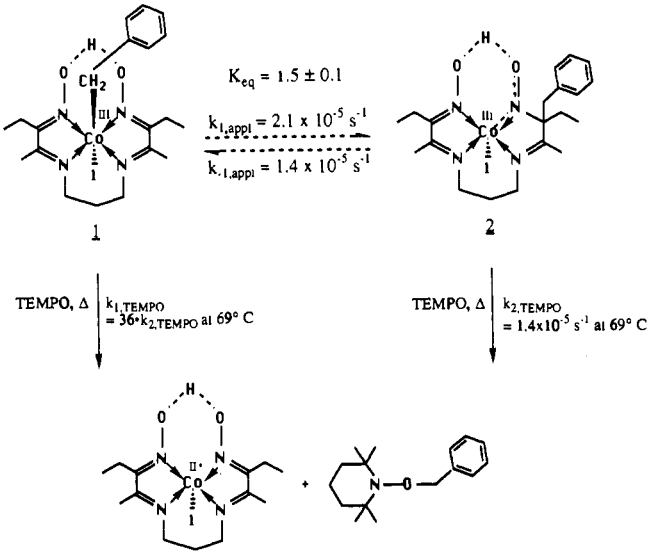

Kinetic Studies. First-order plots of ln ($A_t - A_\infty$) versus time are linear for either the thermolysis of **1** (to give the equilibrium mixture **1** and **2**) or the reverse reaction, the thermolysis of **2** (to give the equilibrium mixture **1** and **2**), Figures 4 and 5. The slopes of the first-order plots are equal to k_{obs}, where $k_{obs} = k_{1,appt} + k_{-1,appt}$ in both cases (appt = apparent).

The mean k_{obs} value was $(3.4 \pm 0.3) \times 10^{-5}$ s^{-1} (four reactions, Table II). This value coupled with $K_{eq} = 1.5 \pm 0.1 = k_{1,appt}/k_{-1,appt}$

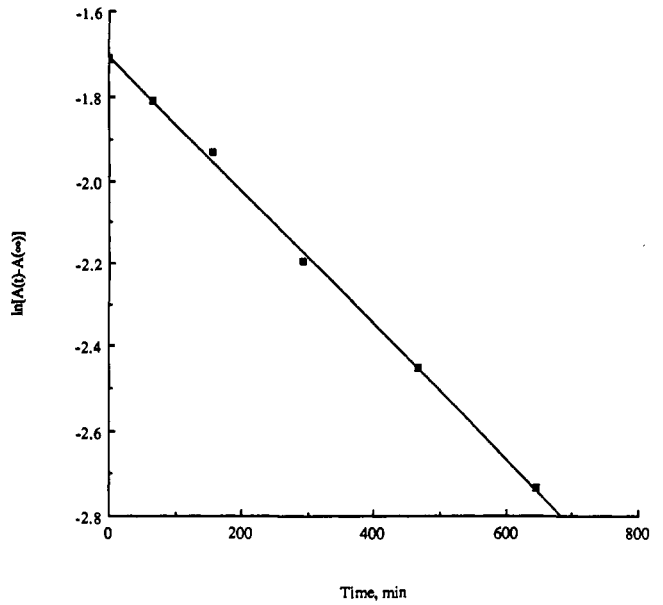

Figure 6. First-order plot of the absorbance for the formation of $^{\bullet}Co^{II}[C_2(DO)(DOH)_{pn}]I$, λ_{max} = 464 nm, from a typical thermolysis reaction of **2** with TEMPO.

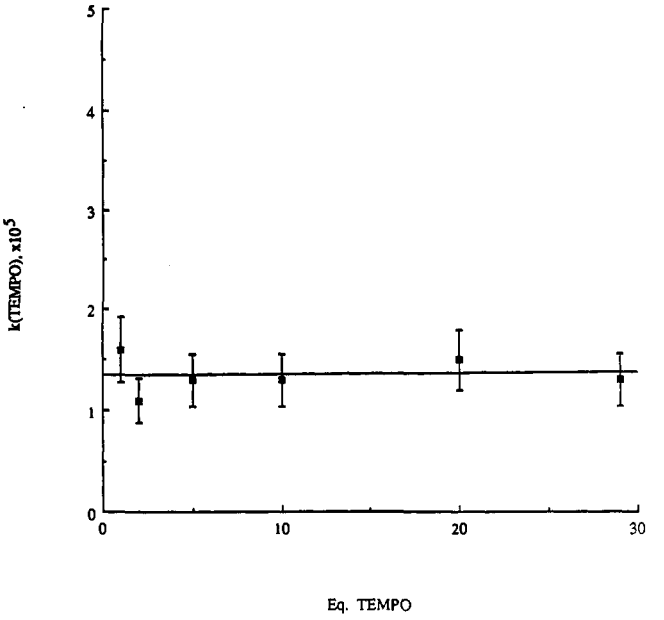

Figure 7. Plot of $k_{2,TEMPO}$ versus equivalents TEMPO. Equivalents of TEMPO, $k_{2,TEMPO}$: 1, (1.6 ± 0.3) × 10^{-5} s^{-1}; 2, (1.1 ± 0.3) × 10^{-5} s^{-1}; (1.3 ± 0.5) × 10^{-5} s^{-1}; 10, (1.3 ± 0.2) × 10^{-5} s^{-1}; 20, (1.5 ± 0.5) × 10^{-5} s^{-1}; 29, (1.3 ± 0.7) × 10^{-5} s^{-1}. Mean $k_{2,TEMPO}$ = (1.4 ± 0.2) × 10^{-5} s^{-1}.

yields $k_{1,appl}$ = (2.1 ± 0.2) × 10^{-5} s^{-1} and $k_{-1,appl}$ = (1.4 ± 0.2) × 10^{-5} s^{-1} (Scheme I). As a check, the raw kinetic data for the thermolysis of either **1** or **2** to the equilibrium mixture of **1** + **2** were integrated numerically by using the GEAR/GIT numerical integration package.[19] The results (Figures B and C, supplementary material) show excellent fits to the data with resultant values of $k_{1,calc}$ = 2.3 × 10^{-5} s^{-1}, $k_{-1,calc}$ = 1.4 × 10^{-5} s^{-1} (average deviation = 3 × 10^{-6}), and $K_{eq,calc}$ = 1.5 ± 0.4 (Figure B, **1** ⇄ **2**) and $k_{-1,calc}$ = 1.4 × 10^{-5} s^{-1}, $k_{1,calc}$ = 2.2 × 10^{-5} s^{-1} (average deviation = 3 × 10^{-6}), and $K_{eq,calc}$ = 1.6 ± 0.4 (Figure C, **2** ⇄ **1**), K_{eq} values within 6% of the previously determined value of 1.5 ± 0.1.

Thermolysis in the Presence of TEMPO. The thermolysis of **2** in the presence of greater than 10 equiv of the radical trap TEMPO (see eq 4) proceeds cleanly with an isosbestic point at 488 nm. (At fewer than 10 equiv of TEMPO, the isosbestic point is not clean as the **2**/**1** equilibrium reaction [$k_{-1,appt}$ = (1.4 ± 0.2) × 10^{-5} s^{-1}] competes, forming **1**, which itself can then undergo thermolysis and TEMPO trapping). The final visible spectrum is identical to the final spectrum of the analogous reaction, thermolysis of **1** in the presence of TEMPO, as both yield $^{\bullet}Co^{II}[C_2(DO)(DOH)_{pn}]I$ and benzylTEMPO[2] as shown in Scheme I above. Authentic benzylTEMPO was synthesized independently and used to calculate the yield (by analytical gas chromatography) of 95 ± 6% benzylTEMPO in the reaction of **2** with TEMPO.

Plots of ln ($A_t - A_\infty$) versus time for these TEMPO thermolysis reactions (with >10 equiv TEMPO) were linear, indicating the reaction is first order overall and thus zero order in TEMPO (a typical plot is shown in Figure 6). Confirming this, the 69 °C thermolysis of **2** with six different concentrations of TEMPO yielded the same rate constant within experimental error indicating that the reaction is indeed rigorously zero order in TEMPO (the plot of $k_{2,TEMPO}$ versus equivalents of TEMPO was linear with a slope equal to zero, Figure 7).[20]

The fact that TEMPO appears in the products but not in the rate law demands the formation of an intermediate (i.e., at least a two-step mechanism). Rate-determining benzyl–carbon bond homolysis in **2** to yield a $PhCH_2^{\bullet}$ free radical intermediate readily accounts for the observed products benzylTEMPO and the stable $^{\bullet}Co^{II}[C_2(DO)(DOH)_{pn}]I$ free radical.

It is important to note that the participation of $PhCH_2^{\bullet}$ and $^{\bullet}Co^{II}[C_2(DO)(DOH)_{pn}]I$ free radicals in the reaction of **2** to **1** is strongly supported by earlier studies,[2] establishing these same two radicals in the thermolysis reaction of **1** with TEMPO to yield (the same products) benzylTEMPO and $^{\bullet}Co^{II}[C_2(DO)(DOH)_{pn}]I$. In that work the rate law was also rigorously zero order in TEMPO, again demanding at least a two-step mechanism, and we were further able in that case to demonstrate an inverse [$^{\bullet}Co^{II}[C_2(DO)(DOH)_{pn}]I$] dependence on the rate. That observation, the products, the rate law, and the direct detection/monitoring of one of the homolysis products ($^{\bullet}Co^{II}[C_2(DO)(DOH)_{pn}]I$) provide the strongest imaginable evidence—short only in direct detection and monitoring of the $PhCH_2^{\bullet}$ intermediate—for reversible homolysis in **1** to $PhCH_2^{\bullet}$ and $^{\bullet}Co^{(II)}[C_2(DO)(DOH)_{pn}]I$ intermediates. This is important, since the principle of microscopic reversibility requires that the conversion of **2** to **1** involves these same intermediates.

When combined, the independent kinetic studies of **1** + TEMPO and **2** + TEMPO provide compelling evidence for rate-determining Co–CH_2Ph and C–CH_2Ph bond homolysis steps, respectively, in the two reactions to common $PhCH_2^{\bullet}$ and $^{\bullet}Co^{II}[C_2(DO)(DOH)_{pn}]I$ intermediates. Restated, beginning with either **1** or **2**, their respective bond homolyses are the kinetically most facile processes.

The intermediacy of a $PhCH_2^{\bullet}$ free radical in the conversion of **2** to **1** is further supported by the finding that $k_{2,TEMPO}$ (i.e., for **2** + ≥10 equiv of TEMPO) is *identical* within experimental error to $k_{-1,appt}$ (**2** being converted to **1**). Given that $k_{2,TEMPO}$ has been demonstrated to involve $PhCH_2^{\bullet}$ and $^{\bullet}Co^{II}[C_2(DO)(DOH)_{pn}]I$ intermediates, the same free radicals *must* be involved in the conversion of **2** to **1** [discounting the conceivable, but unlikely, fortuitous equivalence of $k_{2,TEMPO}$ and $k_{-1,appl}$ for some other reason (i.e., other than their corresponding to the identical chemical step)]. *These kinetic and mechanistic studies, in turn, constitute the first demonstration of a free radical mechanism in such B_{12} model alkyl migration reactions,*[8] ***1*** ⇄ ***2***.

The pseudo-first-order rate constant for the reaction of **2** with TEMPO at 69 °C is $k_{2,TEMPO}$ = (1.4 ± 0.2) × 10^{-5} s^{-1},[21] with one

(19) (a) Numerical integration[19b] presented above was performed with the GEAR[19c] and the GEAR Iterator[19d] (GIT) programs. (b) McKinney, R. J.; Weigert, F. J. *Quantum Chemistry Program Exchange*, Program. No. QCMP022. (c) Stabler, R. N.; Chesick, J. *Int. J. Chem. Kinet.* **1978**, *10*, 461. (d) Weigert, F. J. *Compul. Chem.* **1987**, *11*, 273.

(20) Note that even at very few equivalents of TEMPO, the *observed* rate constant does not (and should not) go to zero as the rate constant for the reaction in the absence of TEMPO ($k_{-1,appt}$) is (1.4 ± 0.2) × 10^{-5} s^{-1} and thus nonzero (see the equilibrium results section).

(21) Rate constants from visible spectroscopy data were determined from absorbance versus time data simultaneously at three different wavelengths, λ = 525, 464, and 340 nm.

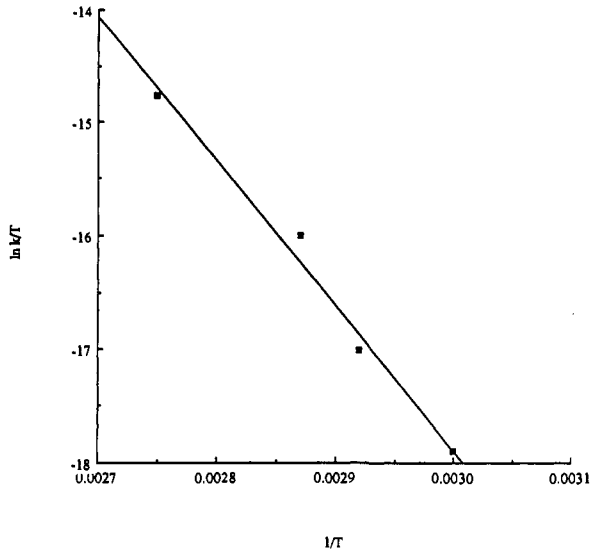

Figure 8. Eyring plot of ln ($k_{2,TEMPO}/T$) versus $1/T$ for four **2** + TEMPO thermolyses over a 30 °C temperature range (60–90 °C).

important point being that $k_{2,TEMPO}$ is 36 times smaller than the pseudo-first-order rate constant for the thermolysis of **1** with TEMPO ($k_{1,TEMPO}$ = 5.0 × 10^{-4} s^{-1}),[2a] Scheme I. Another interesting point is that $k_{1,TEMPO}$ (=5.0 × 10^{-4} s^{-1}) and $k_{1,appl}$ (=2.1 × 10^{-5} s^{-1}) are *not* the same, $k_{1,TEMPO}$ being 24 times larger. Since we previously[2a] established that the cobalt–benzyl bond in **1** homolyses to yield $PhCH_2^{\bullet}$ and $^{\bullet}Co^{III}[C_2(DO)(DOH)_{pn}]I$ free radicals, the implication from the comparison of $k_{1,TEMPO}$ and $k_{1,appl}$ is that these radicals recombine (in the absence of TEMPO) 24 times for each time they go on to yield **2**. Some additional insights that can be gleaned from these rate constant comparisons are deferred until the Discussion section.

An Eyring plot of ln ($k_{2,TEMPO}$) versus $1/T$ for four **2** + TEMPO thermolysis reactions over a 30 °C temperature range gave a linear plot (Figure 8) with $\Delta H^{\ddagger}$ = 26 ± 2 kcal/mol, $\Delta S^{\ddagger}$ = −6 ± 7 cal/(mol·K), or $\Delta G^{\ddagger}_{298}$ = 27 ± 3 kcal/mol.[22] From this $\Delta H_{obs}^{\ddagger}$ measurement a close estimate for the homolytic bond dissociation energy in solution of the benzyl–carbon bond in **2** can be determined. The proper equation for estimating the bond dissociation energy from solution thermolysis measurements is BDE ≃ $\Delta H^{\ddagger}_{obs} - F_c\Delta H^{\ddagger}_{\eta}$, where F_c is the cage efficiency factor and $\Delta H^{\ddagger}_{\eta}$ is the activation enthalpy for viscous flow (and solution effects are assumed to be negligible).[23] Given our finding (see the Discussion section) of an inefficient cage ($F_c \lesssim 0.5$) and computing $\Delta H^{\ddagger}_{\eta} \simeq 2$ kcal/mol for benzene,[23] this equation reduces to BDE ≃ $\Delta H^{\ddagger}_{obs}$ − 1 (±ca. 2) kcal/mol. The resultant benzyl–carbon BDE *estimate* for **2** is BDE ≃ 26 (±2) − 1 (±2) or 25 ± 3 kcal/mol.

This result is quite interesting two reasons. First, the average homolysis BDE for a benzyl–carbon bond is on the order of 76 kcal/mol.[24] Clearly, the BDE of the benzyl–carbon bond in **2** is much less, roughly one-third this value, indicating that *the benzyl–carbon bond in 2 is highly activated.* Second, the *cobalt*–carbon homolysis BDE of **1** was previously determined to be ≃26 ± 1 kcal/mol.[2] *Thus, not only is the benzyl–carbon bond in 2 roughly one-third the average benzyl–carbon bond dissociation energy,*[7b] *it is essentially the same strength (weakness!) as the cobalt–carbon bond in 1.*

Scheme II. (a) Janzen Nitrone[25] Free Radical Trap. (b) Analogous Trapping of the Benzyl Radical by the Nitrone-Like Part of the Ligand in **1** To Form **2**

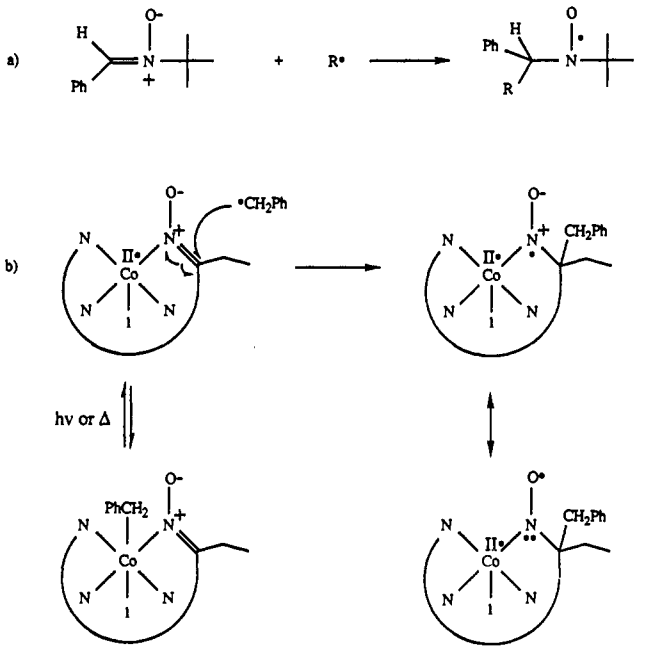

Discussion

Synthetic Chemistry and Structural Findings. The most important finding from our synthetic investigations is that a lower temperature, photochemical route provides the best conversion of **1** to **2**. The single most important *structural* finding from this work is the X-ray diffraction crystal structure, demonstrating a cobalt-to-carbon (and not a cobalt-to-nitrogen)[8-10] migration of the benzyl group. This novel result establishes a firm precedent upon which to reexamine and reformulate the previously reported cobalt-to-nitrogen migrations in B_{12} model complexes.[8,9] This result also indicates an apparent difference between at least porphyrin and corrin or B_{12} model-like systems (and perhaps between porphyrins and corrins themselves).[13]

On close examination of the structure of the starting material **1**, it is perhaps not surprising that the benzyl moiety in the product **2** is trapped at carbon rather than nitrogen. The $CoN^{+}(O^{-})$=CRR′ portion of the ring is very nitrone-like. Nitrones are known to be fast, efficient (10^{6-7} M^{-1} s^{-1}) radical traps, with the trapping occurring at carbon to yield nitroxide products like the general reaction shown in Scheme IIa.[25] Scheme IIb shows the analogous reaction for the conversion of **1** to **2**.

An intriguing question, one not obvious by inspection in this case, is what oxidation state of cobalt is present in **2** (i.e., in its predominant form). Formally, it is Co^{III}, and thus **2** *would appear* to be a rare example of a 5-coordinate, formally Co^{III} B_{12} model complex.[26] Experimentally, the blood-red color of **2** (λ_{max} = 525 nm in benzene) and its closeness to authentic $^{\bullet}Co^{II}[C_2(DO)$-

(22) We considered a mechanism, that could also be zero order in TEMPO, where TEMPO binds to the open coordination site in **2** in a preequilibrium that would have to lie completely to the right to give rise to the observed kinetics. (The significance of such a mechanism is that it would then disallow the connection of the measured $\Delta H^{\ddagger}$ to a benzyl–carbon bond dissociation energy.) To determine if TEMPO could occupy cobalt's empty coordination site in **2**, two types of experiments were undertaken. In the first, a series of visible spectroscopy studies, there was no difference (outside the experimental error of dilution) in the visible spectra of **2** between four different samples with 1, 2, 10, and 20 equiv of TEMPO added. This experiment by itself rules out TEMPO binding with a large equilibrium constant (as required to explain the kinetic studies), except in the unlikely event that **2** and **2**·TEMPO have *identical* visible spectra. In a second independent experiment there was no difference in the ESR spectrum of TEMPO before or after 1 equiv of **2** was added, the sensitive ESR method essentially proving that **2** does not bind the weak ligand TEMPO (see the Experimental Section for further details). Hence, these experiments and the zero-order dependence on [TEMPO] rule out a TEMPO precoordination mechanism.

(23) (a) Koenig, T. W.; Hay, B. P.; Finke, R. G. *Polyhedron* **1988**, *7*, 1499. (b) Koenig, T. W.; Hay, B. P.; Finke, R. G. *J. Am. Chem. Soc.* **1988**, *110*, 2657. (c) Finke, R. G.; Garr, C. D., unpublished results demonstrating the conditions necessary for cage trapping.

(24) McMillan, D. F.; Golden, D. M. *Annu. Rev. Phys. Chem.* **1982**, *33*, 493.

(25) Janzen, E. G.; Evans, C. A.; Davis, E. R. *Organic Free Radicals*; American Chemical Society: Washington, DC, 1978; Vol. 69, p 443. See refs 5 and 6 therein.

(26) (a) Marzilli, L. G.; Summers, M. F.; Bresciani-Pahor, N.; Zangrando, E.; Charland, J.-P.; Randaccio, L. *J. Am. Chem. Soc.* **1985**, *107*, 6880. (b) Hay, B. P.; Finke, R. G. *J. Am. Chem. Soc.* **1987**, *109*, 8012. See ref 25 and references therein.

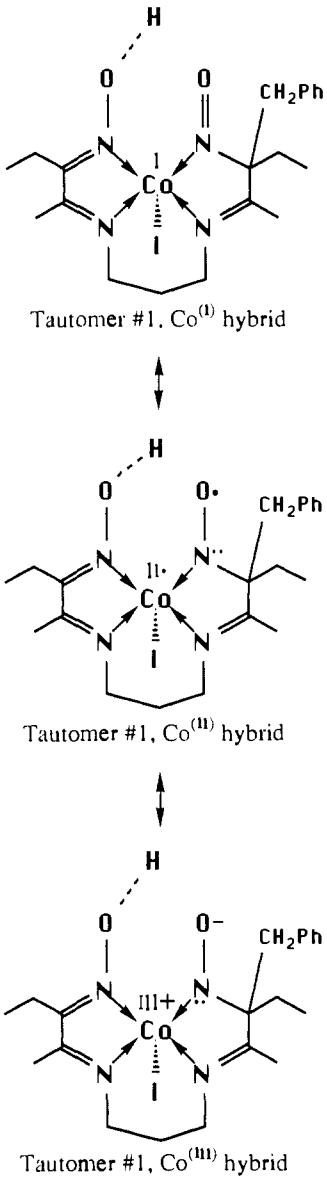

Figure 9. Resonance hybrids of tautomer 1 of **2** showing Co^{I}, Co^{II}•, and Co^{III} hybrids. Note that possible cobalt to N(4) nitrogen double bonding is not shown (but this possibility is indicated by the use of dashed lines in Figure 1).

$(DOH)_{pn}]I$ (λ_{max} = 522 nm in methanol) initially suggested to us (i.e., before the structural characterization) that we had a paramagnetic, Co^{II}• product, but the NMR and lack of an ESR spectrum (for 2 in benzene) show that **2** is diamagnetic (i.e., either Co^{III} or coupled Co^{II}• and ligand• radicals, or possibly Co^{I}). Ultimately, the electronic structure of **2** can be represented[27] as a resonance hybrid of limiting Co^{III}, Co^{II}•, and Co^{I} forms (Figure 9); note that the Co^{II}• (17 electron) and Co^{I} (18 electron) formulations explain the finding of 5-coordinate cobalt.[26]

These resonance hybrids also contain a rationalization for the finding of a very weak, ca. 25 ± 3 kcal/mol benzyl–carbon BDE in **2** as discussed elsewhere.[7b] [Independent confirmation for this result (derived from the thermolysis studies without TEMPO present) is the finding of a $\Delta H \simeq 0$ for the equilibrium **1** ⇌ **2**, confirming that the cobalt–benzyl (in **1**) and the benzyl–carbon (in **2**) BDE's must be essentially the same.] Focusing on the Co^{II}• ligand hybrid form of **2**, one can rewrite the resonance form given previously (the left-most structure below) as a form that puts

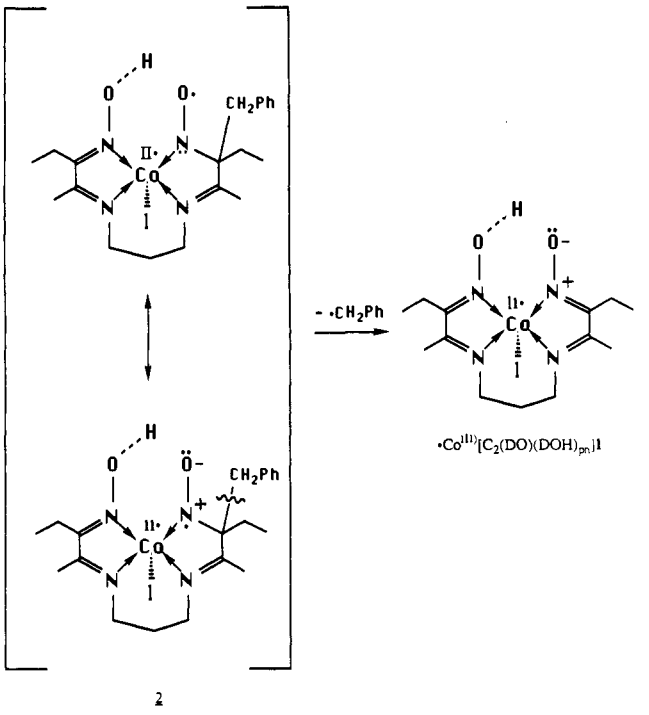

2

Figure 10. Possible cobalt(II) resonance structures for **2** rationalizing a β-scission in **2**, resulting in the homolysis of the benzyl–carbon bond.

unpaired spin density β to the benzyl–carbon bond (Figure 10). β-Scission, a well-established, general type of radical reaction (in the present case of the benzyl–carbon bond as shown), yields two relatively stable *delocalized radicals* (benzyl and $•Co^{II}[C_2(DO)(DOH)_{pn}]I$ radicals). Regeneration of the C=N double bond also helps provide driving force for the β-scission.

Mechanistic Studies. The equilibrium interconversion of **1** ⇌ **2** has also provided an outstanding system for mechanistic investigations, one of the relatively rare systems where the equilibrium constant, its ΔH and ΔS values, *and* the kinetics and activation parameters (and in both directions) have been determined. These values are K_{eq} = 1.5 ± 0.1, ΔH = 0.0 ± 0.2 kcal/mol, ΔS = 0.82 ± 0.06 cal/(mol·K); $k_{1,appl}$ = (2.1 ± 0.2) × 10^{-5} s^{-1}, $\Delta H^{\ddagger}_{1,appl}$ = 27.9 ± 0.8 kcal/mol,[2] $\Delta S^{\ddagger}_{1,appl}$ = 8 ± 2 cal/(mol K),[2] $k_{-1,appl}$ = (1.4 ± 0.2) × 10^{-5} s^{-1}, $\Delta H^{\ddagger}_{-1,appt}$ = 26 ± 2 kcal/mol, and $\Delta S^{\ddagger}_{-1,appt}$ = −6 ± 7 cal/(mol·K).[28] Moreover, as a check for internal consistency of our activation parameters with the independently measured thermodynamic parameters, ΔH and ΔS (and thus ΔG and K_{eq}) were calculated from the above four independently determined activation parameters, $\Delta H^{\ddagger}_{1,appl}$, $\Delta S^{\ddagger}_{1,appt}$, $\Delta H^{\ddagger}_{-1,appl}$, and $\Delta S^{\ddagger}_{-1,appt}$. The calculated values are the same, within experimental error, as the experimentally determined values, lending additional confidence to all the data.[29]

(27) It is conceivable that the true structures differ from the structures shown by having the bridging H predominantly on the right-most oxygen in the structures shown in Figure 9. This should be true, however, only if the Co^{III} hybrid is more important than the Co^{I} hybrid (Figure 9).

(28) (a) The entropy for this step is slightly negative, $\Delta S^{\ddagger}_{-1,appl}$ = −6 ± 7 e.u. (actually, it is zero within experimental error). For comparison, the analogous reaction of **1** with TEMPO yields[2] $\Delta S^{\ddagger}_{1,appl}$ = 8 ± 2 cal/(mol·K). Hence we considered (and have experimentally ruled out, vide infra) a conceivable mechanism where a bimolecular step of solvent coordination to **2** precedes C–CH_2Ph bond homolysis [a mechanism that is perhaps unlikely from the start, given the finding that **2** is stable as a 5-coordinate complex (at least in the solid state) and that our reactions were performed in benzene, a poorly coordinating solvent]. To test this we did two types of experiments. First, the addition of as many as 100 equiv of the coordinating solvent, acetonitrile, to a sample of **2** in benzene yielded no change in the visible spectrum of **2**. Second, the 69 °C thermolysis of **2** with TEMPO plus 100 equiv of acetonitrile demonstrated no rate constant increase (or decrease) for this reaction as would be expected if prior solvent coordination was a key step. Experimental with better coordinating solvents such as pyridine or triphenylphosphine was not attempted as this could result in the displacement of iodine (and thus a change in the overall reaction mechanism). (b) The somewhat negative entropy, $\Delta S^{\ddagger}$ = −6 ± 7 e.u., is in fact expected since two delocalized and thus stiffened[28c] $C_6H_5CH_2$• and $•Co^{II}[C_2(DO)(DOH)_{pn}]I$ rotors are formed, resulting in a loss of vibrational and rotational entropy. (c) Benson, S. W. *Thermochemical Kinetics*, 2nd ed.; John Wiley and Sons: New York, 1976; p 100.

Scheme III. Proposed Mechanism for the Formation of **2**[a]

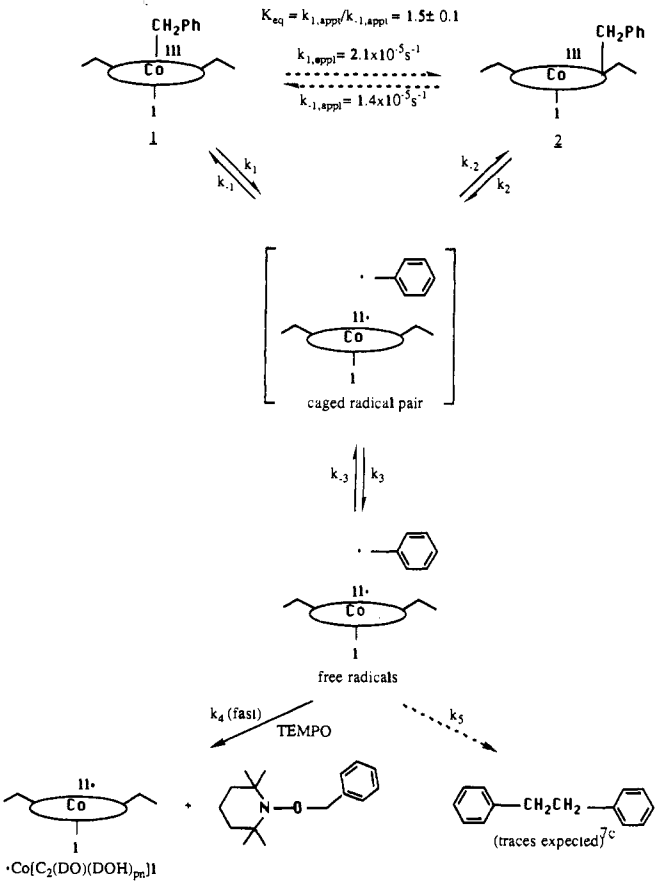

[a] Only the caged radical pair (in brackets) has not been demonstrated as part of these studies.

The most important findings from the above thermochemical data are (1) that the reaction has little driving force, with what there is (ΔG_{342} = −0.28 ± 0.02 kcal/mol) being largely entropic in nature (presumably the greater vibrational and rotational conformational flexibility in **2** compared to **1**);[28b,c] (2) that **2** contains a highly activated benzyl–carbon bond; and (3) that, quantitatively, the benzyl–carbon bond in **2** is ≃ 25 ± 3 kcal/mol, roughly one-third that of a normal benzyl–carbon bond, essentially the same "strength" (really weakness) as the cobalt–benzyl bond on **1**.

The most significant finding from the kinetic studies is the compelling evidence that the reaction of **1** ⇄ **2** proceeds via $PhCH_2^{\bullet}$ and $^{\bullet}Co^{II}[C_2(DO)(DOH)_{pn}]I$ *free radical intermediates*. Recall that the kinetically dominant process in each direction is the production of these free radical intermediates.

The simplest mechanism[30] consistent with all of our experimental data, and with the well-established finding that radical pairs are initially formed in a solvent cage,[23] is that shown in Scheme III. The cobalt–carbon bond (in the case of **1**) or the carbon–carbon bond (in the case of **2**) homolyze, yielding a caged-radical pair for **1** or **2**, respectively (k_1 or k_2).[31] Next, the caged-radical pair can recombine to form either **1** or **2** (k_{-1} or k_{-2}) or escape the cage to form free radicals (k_3) or the reverse process (k_{-3}). If TEMPO trap is present, the benzyl radical can then be irreversibly trapped (k_4), giving benzylTEMPO and $^{\bullet}Co^{II}[C_2(DO)(DOH)_{pn}]I$.

A number of other conclusions and insights are possible regarding Scheme III. Since excess TEMPO radical trap inhibits the formation of **2** from **1** or **1** from **2** (>95%, see supplementary material, Figures C and D) at TEMPO concentrations (≃2 × 10^{-3} M) much less than required for cage trapping,[23c] it follows that cage escape (k_3) is faster than cage recombination to reform **1** or **2** (i.e., $k_3 \gg k_{-1}$ and $k_3 \gg k_{-2}$, at least in the weak-cage solvent used in these studies of benzene at 69 °C). Restated, there is little cage effect and hence it follows that the rate-determining step is homolysis of the cobalt–carbon or benzyl–carbon bonds in **1** or **2**, respectively (k_1 and k_2), and not cage escape (k_3). Next, it is also readily shown that $k_1 = k_{1,TEMPO}$ and $k_2 = k_{2,TEMPO}$ (see the supplementary material for derivations of these and other kinetic equations noted below). Hence, the experimental finding that $k_{1,TEMPO} = 36k_{2,TEMPO}$ means that $k_1 = 36k_2$. The experimental fact that $k_{2,TEMPO} = k_{-1,appl}$ within experimental error means that the inequality $k_{-1} > k_{-2}$ must be true (supplementary material, kinetic derivations, eq 18). Finally, the finding that $k_{1,TEMPO} = 24k_{1,appl}$ allows us to pinpoint that value as $k_{-1} = 24k_{-2}$ (supplemental material, kinetic derivations, eq 19).

An intriguing result, also shown in Scheme III, is that in the absence of trap, bibenzyl is "expected", but none is observed ("none" here means ≤5%, the detection limits of our NMR and GC experiments).[7c] Indeed, the absence of bibenzyl when **1** is thermolysed in the absence of TEMPO trap is another reason we chose to pursue these studies. At first glance the lack of bibenzyl is seemingly contradictory to the mechanism shown in Scheme III, as bibenzyl is a well-known, highly stable recombination product of benzyl radicals. However, Fischer's important work[32] in fact predicts the formation of only trace bibenzyl in the **1** ⇄ **2** interconversion. Fischer's work shows how radical reactions involving two or more intermediates may lead to the specific formation of only one product if one species (i.e., $^{\bullet}Co^{II}[C_2(DO)(DOH)_{pn}]I$ in the present case) is more persistent than the others (i.e., $PhCH_2^{\bullet}$) and if the persistent and transient species are generated with equal rates (as they are here, in both cases, by either Co–CH_2Ph or C–CH_2Ph bond homolysis). This is caused by an initial buildup of the persistent intermediate (due to trace $PhCH_2CH_2Ph$ formation), which then steers the system to follow a single path. Note that Fischer's model predicts *only* trace $PhCH_2CH_2Ph$, consistent with our inability (<5%) to detect it [note that the $^{\bullet}Co^{II}[C_2(DO)(DOH)_{pn}]I$ self-termination Co^{II}–Co^{II} product is unstable since $^{\bullet}Co^{II}[C_2(DO)(DOH)_{pn}]I$ is a stable ("persistent") radical[2]]. The competing reactions are then

$$2Co^{II\bullet} \rightarrow Co^{II}\text{–}Co^{II}\ (k'_2 \simeq 0, \text{ the product is unstable}) \quad (2)$$

$$2C_6H_5CH_2^{\bullet} \rightarrow C_6H_5CH_2\text{–}CH_2C_6H_5\ (k'_3, \text{ very fast}) \quad (3)$$

$$C_6H_5CH_2^{\bullet} + Co^{II\bullet} \rightarrow \mathbf{1} \text{ or } \mathbf{2}\ (k'_4, \text{ fast}) \quad (4)$$

Because it is found experimentally that **1** or **2** is formed quantitatively (±5%), following Fischer's explanation, k'_4 is necessarily greater than the geometric mean of k'_2 and k'_3, and thus eq 4 is the only one to proceed to a significant extent. Since there are few good examples, and even fewer near-ideal systems or *quantitative* investigations of the principles in Fischer's paper, we are investigating the high selectivity (**1** ⇌ **2**) and apparent lack of

(29) (a) From the equations $k = (kT/h)\exp(-\Delta H^{\ddagger} - T\Delta S^{\ddagger})/RT$, $K_{eq} = k_{1,appl}/k_{-1,appl}$, $\Delta G = -RT \ln K_{eq}$, and $\Delta G = \Delta H - T\Delta S$, the four values, K_{eq}, ΔG, ΔH, and ΔS can be determined, given the independently measured values for $\Delta H^{\ddagger}_{1,appl}$, $\Delta S^{\ddagger}_{1,appl}$, $\Delta H^{\ddagger}_{-1,appl}$, and $\Delta S^{\ddagger}_{-1,appl}$. From the limiting cases determined by the uncertainties in the activation parameter values, fairly wide ranges of values for K_{eq}, ΔG, ΔH, and ΔS were obtained, but, in each instance, the experimental values for these parameters fell within the ranges shown below. The calculated ranges were K_{eq} = 0.34–21.8 ($K_{eq,exp}$ = 1.5); $\Delta G_{342,calc}$ = −2.09–0.73 kcal/mol ($\Delta G_{342,exp}$ = −0.28 kcal/mol); ΔH = 0.0 ± 0.2 kcal/mol (assuming a temperature-independent equilibrium, see experimental results); and ΔS_{calc} = −2.1–6.1 e.u. [ΔS_{exp} = 0.82 e.u.].

(30) (a) The probable *slightly* (?) different rates of homolysis of the two tautomeric forms of **2** should be noted but are not included in this simplest mechanism, Scheme III. (b) Bimolecular mechanisms for B_{12} model macrocycle reactions have been reported by Espenson[9a] and Kochi,[9b] but these types of mechanisms predict [**2**]^2 kinetics when *extrapolated* to the present (non-S_H2) system (see Figure F, supplementary material); hence Espenson- or Kochi-type mechanisms can be ruled out in this instance as the thermolyses of both **1** and **2** exhibit first-order kinetics.

(31) At this point, the radical pair is indistinguishable in terms of whether it came from **1** or **2**. It is possible that, when the caged radicals are in close proximity of one another, the benzyl radical occupies an intermediate η^3-benzyl position (or an η^2-benzene position in solution in the ground-state structure of **2**).

(32) Fischer, H. *J. Am. Chem. Soc.* **1986**, *108*, 3925.

bibenzyl formation in greater detail and will report our findings elsewhere.[7c]

Implications for Other Areas and Future Studies. The results presented herein are significant to many facets of both B_{12} model and B_{12}-related chemistry. Certainly the novel structure of the rearrangement product establishes the first firm precedent upon which to reevaluate scattered reports since 1975 of cobalt-to-nitrogen migrations in B_{12} model systems.[8,9] These reports, all of which propose *cobalt-to-nitrogen* migrations, previously borrowed precedent from the ever-growing number of reports of metal-to-ligand *N*-alkyl migrations in a host of different metalloporphyrin cytochrome P-450 model systems.[10] However, the results herein provide the only true precedent for these nonporphyrin cobalt–macrocycle systems and suggest, instead, these literature reports may involve a cobalt-to-*carbon* migration. The present results, and the analogous literature reactions in the cobaloxime B_{12} model system, also bear upon the active area of organic synthesis using cobalt macrocycles as photochemical precursors for R• radicals.[11] Similar products (rather than just Co–R products) are expected, consistent with uncharacterized products seen by others,[11b] in the absence of higher temperatures since the products like **2** should be photostable (to a sunlamp at least). Note that the literature indicates that these possibilities will extend to SALEN and/or SALPHEN systems as well.[9] Furthermore, our studies provide an excellent preliminary[7c] confirmation of Fischer's results,[32] indicating that very selective free radical reactions are possible.

Finally, expanding to what is known about the coenzyme B_{12} cofactor itself, if an analogous reaction can be demonstrated[13] for B_{12},[33] then a speculative, but intriguing, possibility emerges: B_{12} might never generate a protein-bound 5′-deoxyadenosyl radical *as a distinct intermediate*, since such a side reaction with the corrin ring would limit the number of catalytic turnovers. (This idea is fully consistent both with the failure of anyone to observe an Ado• radical in the functioning enzyme[34] and with the proposed protein-S• radical-chain mechanism.[35]) Alternatively, the absence of such a migration in B_{12} itself (which lacks the nitrone-like functionality present in **1**) would lead to the speculation that one advantage (among others)[36] of having a corrin rather than a porphyrin ligand in B_{12} is the greater inertness of a corrin to such alkyl migration reactions (and probably to radical reactions in general). These ideas are presently under investigation.[13]

Experimental Section.

General. Reagents. Unless otherwise noted, all laboratory reagents were used as received without further purification. Benzene was distilled under N_2 over CaH_2. Deuteriobenzene (99.6% D), Cambridge Isotopes, was degassed by bubbling with N_2 for 30 min. TEMPO free radical (Aldrich) was purified by water aspirator vacuum sublimation at ambient temperature (mp = 36–38 °C, lit. = 37–39 °C).[37] Benzyl Iodide (ICN Biomedicals Inc., K & K Labs) was also purified by water aspirator vacuum sublimation. It gave a satisfactory NMR spectrum and was bubbled with N_2 for 30 min before use. Carbon monoxide and house nitrogen were scrubbed for water (4-Å molecular seives) and O_2 (BASF copper catalyst in the black, reduced form).

Equipment. Proton NMR spectra, referenced to the benzene protic impurity, δ 7.15, were recorded on GE QE-300 and GN 500-MHz spectrometers. Ultraviolet and visible spectra were measured by using a Beckman DU-7 spectrometer. Infrared spectra were measured on a Nicolet 50XB FT-IR spectrometer. Preparative gas chromatography was done on a Varian Aerograph Series 2700 gas chromatograph with a 1.5% 100/120 OV-101 column. Analytical gas chromatography was done with a Hewlett-Packard 5790A Series GC with an Alltech Econo-cap carbowax capillary column, 30 m × 0.25 mm i.d., film thickness = 0.25 μm. Mass spectra were recorded on a VG-12-250 mass spectrometer, 70-eV positive/ion mass spectrum. ESR spectra were recorded on a Bruker ESP 300 electron spin resonance spectrometer. X-ray crystallographic data were collected on a Rigaku AFC6R diffractometer. Conductivities were measured on a YSI Model 31 conductivity bridge, using probes with cell constants k = 0.1, 1, and 2 cm^{-1}.

Air-Sensitive Technique. All air-sensitive compounds were manipulated either by Schlenk technique or in an inert atmosphere, double-length, nitrogen-containing glovebox (Vacuum Atmospheres). Oxygen levels averaged 0.3 ppm and did not exceed 2 ppm. Air-free transfers outside the box were done by either gas-tight syringe or stainless steel cannula. Spectra of air-sensitive compounds were taken in either Pyrex cuvettes fitted with airtight Teflon screw caps (Kontes) or NMR tubes fitted with airtight Teflon screw caps (J. Young).

Light-Sensitive Technique. All light-sensitive compounds were protected from exposure to light by wrapping their containers with either aluminum foil or black electrician's tape. Transfer of these compounds was done in the near dark, in a dark room, or in a hood shrouded with black curtains, with minimal exposure to room light.

Quenching Technique. All cuvettes and NMR tubes containing samples used in thermolysis reactions (60–90 °C) were first quenched by cooling in room temperature water for at least 5 min before spectra were taken.

Internal Standards. In order to authenticate the NMR integrals used in the equilibrium measurements and to verify that the sum of the two species, **1** and **2**, was remaining constant throughout the experiments, an internal standard was required. Triphenylmethane, Ph_3CH (TPM), proved to be a convenient internal standard due to its singlet at δ 5.14, where no peaks from **1** or **2** appear. In addition it is stable and unreactive toward **1** and **2**.

T_1 Experiments. To authenticate the NMR integrals used in all subsequent kinetic studies performed on **1** and **2**, the aquisition times used in the NMR experiments were shown to be long enough so that the downfield protons have adequate time to relax between pulses, thereby giving accurate integral values. For a 1-s relaxation period, the mean fraction of **1** [i.e., $1/(1 + 2)$] was found to be 0.22 ± 0.03. The mean fraction of **1** for a 10-fold longer relaxation time was found to be 0.20 ± 0.02. Hence, within experimental error, the fraction of **1** at two 10-fold different relaxation times is constant, and thus the default delay time of 1 s is sufficient to give reliable NMR integrals.

Preparation of Compounds. (OC)Co^{I}[C$_2$(DO)(DOH)$_{pn}$]. Air-sensitive (trimethylenedinitrilo)bis(3-oximato-2-pentanone)cobalt(I) was prepared by our literature method.[6a] Under reducing conditions and in especially designed Schlenkware,[6a] CO was bubbled through a solution of Co^{III}[C$_2$(DO)(DOH)$_{pn}$]I$_2$ in 10% MeOH/NaOH. After the solution bubbled for 1 h, the solvent was pumped off under vacuum and the brown microcrystalline product was washed with water, dried, and collected. Yields for three separate preparations were 0.75–1.05 g (49–70%). Purity was determined to be >95% by NMR in agreement with the literature.[6a] Anal. Calcd: C, 47.4; H, 6.5; N, 15.8. Found: C, 46.58; H, 6.35; N, 15.75. Carbon consistently gives a poor analysis for this partially H_2O-solvated, air-sensitive compound. However, it is pure enough to consistently give analytically pure products, including the following synthesis.[6a]

C$_6$H$_5$CH$_2$Co^{III}[C$_2$(DO)(DOH)$_{pn}$]I (1). *trans*-Benzyliodo(trimethylene-dinitrilo)-bis(3-oximato-2-pentanone)cobalt(III) was prepared via a modification of our previously reported synthesis.[2] In the drybox, three to five equivalents of benzyl iodide were added to a solution of Co^{I}[C$_2$(DO)(DOH)$_{pn}$]CO in benzene. The benzyl iodide oxidatively adds to the Co^{I}[C$_2$(DO)(DOH)$_{pn}$]CO virtually instantaneously as judged by the blue-to-brown color change. (It is important *not* to cap the flask so that the CO produced can escape; otherwise the reaction will not proceed to completion.) Yields for four separate preparations were 0.40–0.96 g (50–95%). Purity was determined to be >95% by NMR and visible spectroscopy. ^{1}H NMR (benzene-d_6; peak assignments are supported by 1D decoupling and 2D-COSY experiments) δ 0.9 (t, 6 H), 1.2 (s, 6 H), 1.5 (m, 1 H), 2.2 (m, 2 H), 2.5 (s, 2 H), 2.6 (m, 4 H), 3.4 (m, 3 H), 6.7 (t, 2 H), 6.8 (t, 2 H), 6.9 (t, 1 H), 20.2 (s, 1 H). ^{13}C NMR (benzene-d_6) δ 9.8 (s, 2 C), 16.4 (s, 2 C), 20.2 (s, 2 C), 28.7 (s, 1 C), 37.9 (m, 1 C), 48.8 (s, 2 C), 124.7 (s, 1 C), 128.2 (s, 4 C), 146.4 (s, 1 C), 157.5 (s, 2 C), 169.7 (s, 2 C). Anal. Calcd for C$_6$H$_5$CH$_2$Co[C$_2$(DO)(DOH)$_{pn}$]I: C, 44.1; H, 5.5; N, 10.3. Found: C, 44.15; H, 5.44; N, 10.18.

Co^{III}[C$_2$(DO)(DOH)$_{pn}$CH$_2$Ph]I, (*SP*-5-15)-[2-[[3-[[2-(Hydroxyamino)-1-methyl-2-(phenylmethyl)butylidene]amino]propyl]imino]-3-pen-

(33) Perhaps the most intriguing report is from Hogenkamp who writes (see eq 16, p 420) a $RCH_2^•$ (R = H) addition to the corrin ring in the photolysis of MeB_{12} in the presence of trace O_2: Hogenkamp, H. P. C. *Biochemistry* **1966**, *5*, 417. This report is currently being reinvestigated.[13]

(34) Babior, B. M.; Krouwer, J. S. *CRC Crit. Rev. Biochem.* **1979**, *6*, 35 and references therein.

(35) (a) Cleland, W. W. *Crit. Rev. Biochem.* **1982**, *13*, 385. (b) Stubbe, J. *Mol. Cell Biochem.* **1983**, *50*, 25. (c) McGee, D. Ph.D. Dissertation, California Institute of Technology, Pasadena, CA, 1983. (d) O'Brien, R. J.; Fox, J. A.; Kopczynski, M. G.; Babior, B. M. *J. Biol. Chem.* **1985**, *260*, 16131. (e) Ashley, G.; Stubbe, J. *Pharmacol. Ther.* **1987**, *30*, 301. (f) Stubbe, J. *Biochemistry* **1988**, *27*, 3893.

(36) Halpern and Geno (Kendrick) have convincingly demonstrated that a corrin's greater flexibility is another reason why B_{12} has evolved to contain a corrin rather than a porphyrin: Geno (Kendrick), M. J.; Halpern, J. *J. Am. Chem. Soc.* **1987**, *109*, 1238.

(37) Rozantzev, E. G.; Nieman, M. B. *Tetrahedron* **1964**, *20*, 131.

tanone oximato(2−)-*N*,*N*′,*N*″,*N*‴]iodocobalt(III) (2). In the drybox 197 mg of **1** were dissolved in 95 mL of benzene in a 300-mL round-bottom flask fitted with a rodaviss joint[38] without grease. The flask was sealed and brought out of the box. The flask was secured above a foil plate, 30 cm below a 275-W GE sunlamp. Room-temperature air was blown over the flask continually. The flask was photolysed for about 48 h. The flask was taken back into the box and 5 mL was removed and rotoevaporated to dryness. The dry product was dissolved in about 2 mL of deuterated benzene and transferred to and sealed in an air-tight NMR tube. Evaluation by NMR showed the reaction to be complete. The benzene was removed by rotoevaporation outside the box. The product was scraped out of the flask, placed in an amber vial, aerated with N_2 for 30 min, and placed in the freezer. All preparations showed 100% reaction by NMR (**1** peak at δ 20.24 completely gone), but it was difficult to collect all of the product due to static electricity in the drybox, thus the lower isolated yields (for six separate preparations), 0.047–0.12 g (23–54%). ^{1}H NMR (benzene-d_6; assignments are supported by 1D decoupling and 2D COSY experiments) δ 1.1 (m, 6 H), 1.2 (m, 3 H), 1.3 (m, 3 H), 1.6 (m, 2 H), 1.9 (d, 1 H), 2.6 (m, 2 H), 2.8 (m, 2 H), 2.9 (m, 2 H), 3.1 (m, 1 H), 3.3 (m, 1 H), 4.3 (t, 1 H), 6.1 (d, 2 H), 6.7 (m, 3 H), 17.5 (s, 1 H). ^{13}C NMR [benzene-d_6; assignments are supported by ATP (attached proton test) experiments] δ 10.32 (C_9), 11.00 (C_{13}), 15.32 (C_{10}), 16.66 (C_{11}), 21.20 (C_{14}), 26.93 (C_4), 30.14 and 38.08 (C_3 and C_5), 49.84 (C_8), 50.37 (C_{12}), 126.44, 127.01, 129.29 (C_{15}–C_{20}), 161.74 (C_1 and C_7), 176.60 (C_2 and C_6).[39] Anal. [Vacuum dried (6 h, 25 °C), benzene solvate free sample] calcd for $C_{20}H_{30}N_4O_2ICo$: C, 44.1; H, 5.5; N, 10.3. Found: C, 43.88; H, 5.47; N, 9.50 (repeat anal.: C, 43.91; H, 5.46; N, 9.64). Mass spectrum: *m*/*e* (relative intensity; assignment) 544 (0.43; M^+, parent ion), 528 (0.40; $M^+ - O$), 453 (0.37; M^+ − benzyl), 91 (100; benzyl$^+$; base peak).

2,2,6,6-Tetramethyl-1-(benzyloxy)piperidine, benzylTEMPO, was prepared by a combination of literature methods.[2,4d,e] A 250-mL one-neck round-bottom flask equipped with a pressure-releasing addition funnel was taken through three cycles of vacuum purging and back-filling with N_2. Twenty milliliters (40 mmol) of 2.0 M benzyl magnesium bromide in THF (Aldrich) was then added, followed by 20 mL of degassed ether. In a separate flask, 14.58 g (93 mmol; ≥2 equiv) of sublimed TEMPO was dissolved in 20 mL of degassed ether. The TEMPO solution was transferred by needlestock to the addition funnel. The Grignard solution was cooled to −10 °C with a salt water bath and the TEMPO solution was added dropwise over 1 h while the mixture was stirred by magnetic stir bar until the orange color persisted indicating excess TEMPO. The mixture was a cloudy orange, the cloudiness due to insoluble $MgBr_2$. The mixture of benzylTEMPO and TEMPO$^-$ $MgBr^+$ products was exposed to the atmosphere and 20.3 g of NH_4Cl in 100 mL of distilled water was added. The precipitate dissolved and the solution turned dark orange. Two immiscible layers became visible. The solution was allowed to warm to room temperature and was placed in a 250-mL separatory funnel. The aqueous layer was removed and the organic layer washed with distilled water (125 mL, 2 times). The organic solution was then transferred to a 150-mL Erlenmeyer flask and dried overnight with $MgSO_4$. The next day, the solution was placed first under a vacuum aspirator and then high vacuum to remove the volatile solvents, ether, and THF. The desired product was purified to approximately 90% purity (by NMR) by using preparative gas chromatography (column conditions: 1.5% OV-101, 100/120, injector 185 °C, detector 225 °C, column 130–200 °C). A total of six peaks were seen by GC and were determined to be ether, toluene, THF, TEMPO (oxidized TEMPO$^-$ $MgBr^+$), bibenzyl, and benzylTEMPO in that order. BenzylTEMPO was the largest peak and made up approximately 60–70% of the total crude mixture. The total yield of the preparation was not determined, as only enough product as was needed for further experiments was collected (about 500 μg). Ideally, it would have been best to have a sample of pure benzylTEMPO, as it was used to quantify the amount produced in the **2** + TEMPO thermolysis reaction. However, even upon 3-fold preparative GC purification of a sample of benzylTEMPO, a small amount of TEMPO and bibenzyl are found (these are the decomposition products of benzylTEMPO[6a]). Adjusting the column temperatures did not help as, at lower temperatures, the bibenzyl and benzylTEMPO peaks begin to broaden and blend together. This problem was solved simply by quantifying the amount of bibenzyl, TEMPO, and benzylTEMPO in the purified mixture by analytical gas chromatography. ^{1}H NMR (acetonitrile-d_3) δ 1.1–1.5 (m, 18 H), 4.78 (s, 2 H), 7.36 (m, 5 H) (in agreement with literature values).[40] Mass spectrum: *m*/*e* (relative intensity; assignment) 247 (11; M^+, parent ion), 91 (47; benzyl$^+$), 156 (100; TEMPO$^+$).

Product Studies. X-ray Structural Analysis of 2·0.5C_6H_6. Red-black lath-shaped crystals of 2·0.5C_6H_6 were grown from O_2-free benzene solution, washed with hexane, and sucked dry on a glass frit in the glovebox and then sealed in Lindemann glass capillaries outside the box. Intensity data were obtained from one crystal at Molecular Structures Corporation, College Station, TX, after cell dimensions had been calculated from the setting angles of 23 centered reflections in the range $20.1 \geq 2\theta \geq 24.1°$. Crystal parameters and particulars of data collection and refinement are given in Table I and the supplementary material of our earlier paper.[7a] Because the crystal diffracted weakly, only 51% of the independent reflections scanned were observed, but no problems were experienced during the structure analysis. The TEXSAN program suite,[41] installed on a MicroVAX II/RC computer at Oregon State University, was used in all calculations. The distribution of intensities was clearly centric. The approximate positions of the iodine and cobalt atoms were obtained from a Patterson synthesis. All other non-hydrogen atoms, including the three independent carbon atoms of a molecule of benzene solvate, were located from a single cycle of DIRDIF.[42] All non-hydrogen atoms other than the benzene atoms C(21,22,23) were allowed anisotropic thermal parameters in the later cycles of full-matrix least-squares refinement, and hydrogen atoms were included at calculated positions with *B* values constrained to 1.2 times the values of B_{eq} for the parent atoms. The maximum deviation from planarity in the final difference synthesis was +0.90 e Å^{-3}, about 1.0 Å from the iodine atom. Scattering factors were taken from refs 43 (H) and 44 (other atoms). The following have already been published and are available as supplementary material to our preliminary paper:[7a] details of the X-ray structure analysis of 2·0.5C_6H_6; an ORTEP diagram; tables of refined atomic coordinates, bond lengths, and angles; calculated hydrogen atom coordinates; and anisotropic thermal parameters (12 pages). Also available are observed and calculated structure factors (16 pages).[7a]

Photolysis of 1 at Low (UV/Visible; ca. 10^{-4} M) Concentrations. In the drybox 30 mg (0.055 mmol) of **1** was dissolved in 10.0 mL of benzene. A 0.20-mL sample of this solution was diluted to 10.0 mL with benzene to yield a final [**1**] = 1.1×10^{-4} M. A visible cuvette was filled with this solution, covered with foil, and brought out of the box. The contents of the cuvette were photolyzed with a 275-W GE sunlamp placed 30 cm from the cuvette, which was placed on a reflective foil plate. The reaction was followed periodically by visible spectroscopy.

2 + TEMPO Thermolysis, GC Product Analysis. In the drybox 3.3 mg of **2** was dissolved in 0.60 mL of benzene in an airtight NMR tube. TEMPO (32 mg; 34 equiv) was added to the tube. The tube was sealed, protected from light with aluminum foil, and removed from the box and the contents were thermolysed for about 28 h in a 69.0 ± 0.2 °C oil bath. The tube was removed from the bath and taken back into the box where 1.4 mL of heptane was added. The solution was transferred to a 3-mL vial, capped with a septum, and removed from the box for GC analysis.

Experiments Designed To Test Tautomerization versus Other Conceivable Explanations for the Two Downfield ^{1}H NMR Peaks in 2. 500-MHz NMR of 2. In the drybox, 47 mg of **2** was dissolved in 2 mL of deuteriobenzene. The solution was filtered through glass wool into an airtight NMR tube and sealed. The tube was brought out of the box and subsequently analyzed by 500-MHz NMR to examine the hydroxylic protons of **2** that appear at δ 17.47 and 17.37. A careful search of the remainder of the entire 500-MHz NMR spectrum of **2** was done to see if it revealed any of the splitting expected of the other peaks *if* the two downfield peaks were due to the presence of diastereomers of **2** or if the I^- was dissociating. No such splitting was observed.

NMR Analysis of Crystalline 2 in Protic and Polar Nonprotic Solvents. The series of ^{1}H NMRs of **2** described below (in benzene, chloroform, acetone, methanol, dimethyl sulfoxide, and acetonitrile) revealed that only in benzene are the two downfield proton peaks visible[17b] [solvent,

(38) The rodaviss joint (purchased from Witeg) is a typical ground-glass joint (24/14 in this case) but with screw threads on the outside of the female end. The glass stopper has a flange that a rubber O-ring butts up against. An open plastic screwcap fits down over the top, sealing the flask when tightened down over the O-ring.

(39) ^{1}H and ^{13}C NMR peak assignments for **2** are similar to those documented in similar compounds. Parker, W. O., Jr.; Zangrando, E.; Bresciani-Pahor, N.; Marzilli, P. A.; Randaccio, L.; Marzilli, L. G. *Inorg. Chem.* **1988**, *27*, 2170.

(40) Johnston, L. J.; Tencer, M.; Scaiano, J. C. *J. Org. Chem.* **1986**, *51*, 2806.

(41) TEXSAN *Texray Structural Analysis program suite*, Molecular Structures Corporation, College Station, TX, 1987.

(42) Buerskens, P. T. *DIRDIF: Direct Methods for Difference Structures*, Technical Report 1984/1, Crystallographic.

(43) Stewart, R. F.; Davidson, E. R.; Simpson, W. T. *J. Chem. Phys.* **1965**, *42*, 3175.

(44) Cromer, D. T.; Waber, J. T. In *International Tables for X-ray Crystallography*; Kynoch Press: Birmingham, England, 1974; Vol. I, pp 71, 148.

chemical shift; C_6D_6 δ 17.47 and 17.37; $CDCl_3$, δ 16.42; $(CD_3)_2CO$, δ 16.67 (no visible H/D exchange after 24 h); $(CD_3)_2SO$, δ 16.29; CD_3OD, no peaks (H/D exchange); CD_3CN, δ 16.26]. The experiments were performed as follows. Crystals of **2** (ca. 2 mg) were dissolved in 0.50 mL of acetone-d_6 in an airtight NMR tube in the drybox. The tube was sealed and removed from the box and a ^1H NMR was taken with an emphasis on the downfield peaks at δ 17.47 and 17.37. The acetone ws removed under vacuum, and the precipitate was redissolved in methanol-d_4 in the box. Again, the tube was sealed and removed from the box and the same two peaks were examined in the ^1H NMR. Two to four milligrams of crystals of **2** was dissolved in 0.6 mL of $CDCl_3$ in an airtight NMR tube in the box. The tube was sealed and removed from the box and an ^1H NMR was similarly taken. The $CDCl_3$ was removed under vacuum as before and the product was redissolved in a similar volume of CD_3CN in the drybox. The tube was removed from the box and again analyzed by ^1H NMR. Two to four milligrams of crystals of **2** was dissolved in 0.8 mL of DMSO-d_6 in the box. The NMR tube was sealed and removed from the box and the sample analyzed by ^1H NMR. The DMSO was removed under vacuum, and the product was redissolved in benzene-d_6 in the box. The tube was again sealed and removed from the box and the sample analyzed by ^1H NMR.

Variable-Temperature ^1H NMR of 2. In the drybox, 5 mg of **2** was dissolved in 1 mL of benzene-d_6 in an airtight NMR tube. The tube was sealed and removed from the box and the sample analyzed by variable-temperature NMR. The sample was cooled to 7.5 °C inside the probe and an NMR was taken. The sample was then warmed progressively and NMRs were taken over a series of temperatures (7.5, 10, 15, 20, 30, 40, 50, 70, and then back to 30 °C). The peaks of interest, at δ 17.47 and 17.37, were examined as a function of temperature to determine if the presumed tautomerization between these two peaks is temperature-dependent. In fact, this experiment demonstrated that the two peaks coalesce fully by 70 °C and return to the original 2 peaks by 30 °C.

Conductivity Measurements. In the drybox 4.5×10^{-4} M solutions of $Bu_4N^+I^-$, $ICo^{III}[C_2(DO)(DOH)_{pn}]I$, and **2** in acetonitrile and benzene were prepared. The conductance (L) of each solution was measured and, from these values, the molar conductivity (Λ) of each solution was determined.[45] The goal of this experiment was to determine whether or not I^- dissociation in **2** in benzene could explain the presence of the two downfield proton peaks in the ^1H NMR of **2** in that solvent. These conductivity measurements of $ICo^{III}[C_2(DO)(DOH)_{pn}]I$ or **2** in acetonitrile and benzene, relative to $Bu_4N^+I^-$, a known 1:1 electrolyte, revealed that in acetonitrile $ICo^{III}[C_2(DO)(DOH)_{pn}]I$ is ≃12% dissociated while **2** is ≃62% dissociated. *However, and as expected, there was no detectable conductivity (<0.0004 Ω^{-1} cm^{-1} M^{-1}) for any of these compounds in benzene.* Thus, I^- dissociation cannot explain the two downfield ^1H NMR peaks as there is no detectable conductivity in the only solvent (benzene) to show the two downfield peaks in the ^1H NMR of **2**, a result that rules out possibilities 2 and 3 discussed in footnote 16.

IR Analysis of 2. In the drybox 5 mg of **2** was mixed in a mortar with 100 mg of oven-dried, powdered KBr. The powdered mixture was removed from the box and a portion was pressed into a pellet, which was subsequently analyzed by IR. A saturated solution of **2** in benzene was also prepared in the drybox. A portion of this solution was placed in a solution IR cell, removed from the box, and subsequently analyzed by IR versus a benzene blank. The solid-state IR spectrum of **2** revealed one broad, intense O–H stretch in the bridging O··H··O region (≈3460 cm^{-1}), while even a saturated solution of **2** in benzene was not concentrated enough to detect a solution IR spectrum. Thus IR was not an effective method for testing the tautomer explanation or for comparing solution IR and NMR data.

Equilibrium and Kinetic Studies. Determination of T_1 Relaxation Time. A few milligrams of **1** was dissolved in 1 mL of deuterated benzene in an airtight NMR tube (the solution was less than saturated). The contents of the tube were thermolysed at 70 °C for about 3 h to produce some **2**. The reaction was quenched and three NMRs were taken. A relaxation time of 1 s was used and the magnet was shimmed between each NMR. The two downfield protons corresponding to **1** and **2** were integrated versus TMS internal standard and the fraction of **1** [**1**/(**1** + **2**)] was calculated. Three more NMRs were taken, this time with a longer relaxation time of 10 s, and again the magnet was shimmed between each NMR. Again the two downfield protons were integrated and the fraction of **1** [**1**/(**1** + **2**)] was again calculated.

Thermolysis of 1 at Higher (NMR) Concentration with Ph_3CH Internal Standard. In the drybox 9.67 mg (0.0178 mmol) of **1** and 2.45 mg (0.0100 mmol) of triphenylmethane (TPM) were dissolved in 1.25 mL of deuterated benzene in an airtight NMR tube. [**1**] = 1.42×10^{-2} M; [TPM] = 8.02×10^{-3} M. The contents of the tube were thermolysed at 69.0 ± 0.2 °C and the reaction was followed by NMR.

Thermolysis of 2 at Higher (NMR) Concentrations with Ph_3CH. The tube from the above reaction was photolysed to pure **2** (clean NMR with good resolution). The contents of the tube were then thermolysed at 69.0 ± 0.2 °C and the reaction was followed by NMR.

Visible Spectroscopy Evaluation of 1 Thermolysis at Higher (NMR) Concentrations. In order to prove that $^{\bullet}Co^{II}[C_2(DO)(DOH)_{pn}]I$ and ≥5% of bibenzyl are not formed in the thermolysis reaction at higher (NMR versus UV/visible concentrations), a visible spectrum of the equilibrium product mixture was necessary. By comparing the equilibrium mixture spectrum to that of a mathematically weighted spectrum of 40% **1** and 60% **2**, and the photolysed product spectrum to that of authentic **2**, it is possible to determine whether or not the thermolysis of **1** or **2** to the equilibrium mixture and subsequent photolysis to **2** are quantitative (≥95%) reactions. Complex **1**, 4.89 mg (0.00898 mmol), was dissolved in 1.25 mL of deuterated benzene. No internal standard was used to avoid interference with the visible spectrum; [**1**] = 7.19×10^{-3} M. The contents of the tube were thermolysed as before at 69.0 ± 0.2 °C for about 42 h. Subsequent NMR showed that the reaction had reached equilibrium (39 ± 2% **1** by integration). The tube was taken into the box and a few drops of the reaction mixture were placed in a visible cuvette with benzene. This was all done with protection from light to prevent the reaction from continuing further. The cuvette and NMR tube were both sealed and a visible spectrum of the cuvette was taken. The contents of the NMR tube was then photolysed until the reaction was complete. The tube was taken back into the box and another cuvette of the reaction mixture was made up. A visible spectrum of this cuvette was taken as well. Indeed, the equilibrium spectrum matched the weighted **1**/**2** spectrum and the photolysed product spectrum matched the spectrum of authentic **2**.

Thermolysis of 1 and 2 at Lower (UV/Visible) Concentrations. It is interesting and important to know whether the thermochemical formations of **2** from **1** and **1** from **2** are clean reactions at lower concentrations as well. In the drybox 6.3 mg of **1** was dissolved in 10.0 mL of benzene. 0.3 mL of this solution was diluted to 3.0 mL ([**1**] = 1.2×10^{-4} M). This solution was placed in a visible cuvette and brought out of the box, and the contents were thermolysed in the dark at 69.0 ± 0.2 °C for about 8 h. The reaction was followed to completion (until no change in consecutive spectra was observed) by visible spectroscopy. The contents of the cuvette were then photolysed for 40 min and monitored by visible spectroscopy until the reaction was complete. Finally, the contents of the cuvette were again thermolysed at 69.0 °C for about 29 h until the reaction was complete. The 69 °C thermolysis of **1** at low concentration was clean by visible spectroscopy, giving an isosbestic point at 466 nm. Again, the final spectrum matched that of the mathematically weighted spectrum of 40% **1** plus 60% **2**. Photolysis of this equilibrium mixture proceeded cleanly through the same isosbestic point at 466 nm and the final spectrum was that of **2** with λ_{max} at 525 nm. Thermolysis of this solution again proceeded cleanly with an isosbestic point at 466 nm and the final spectrum matched the same 40/60 weighted spectrum.

Simultaneous Photolysis/Thermolysis of 2 at Lower (UV/Visible) Concentrations. In the drybox 5.0 mg of **1** was dissolved in 10.0 mL of benzene. A 0.3-mL sample of this solution was diluted to 3.0 mL ([**1**] = 9.2×10^{-5} M). This solution was placed in an airtight cuvette, sealed, and brought out of the box, and the contents were photolysed while submerged in an oil bath at 69.0 ± 0.2 °C. The reaction was followed by visible spectroscopy to completion (ca. 69 min). The simultaneous photolysis/thermolysis of **1** also proceeded cleanly with an isosbestic point at 466 nm. However, under these conditions, the reaction produced 100 ± 5% **2** rather than the 40/60 *thermolysis* equilibrium mixture of **1** and **2**.

85 °C Thermolysis of 1 at Higher (NMR) Concentrations. In the drybox about 5 mg of **1** was dissolved in 1 mL of deuterated benzene in an airtight NMR tube. The tube was removed from the box and the contents thermolysed for about 36 h at 69.2 ± 0.2 °C to produce the known **1**/**2** equilibrium mixture. The tube was then thermolysed for an additional 48 h at 85 ± 2 °C. At the end of this time, the tube was quenched and ^1H NMRs were taken. The goal of this experiment was to evaluate the equilibrium constant at a temperature other than 69 °C. Indeed, at this temperature, the **1**/**2** ratio was the same as that at 69 °C within experimental error (2%). However, at this higher temperature the peaks in the ^1H NMR were broadened, resolution was poor, and precipitate had formed in the tube. Clearly some decomposition had occurred and likely some $^{\bullet}Co^{II}[C_2(DO)(DOH)_{pn}]I$ was formed.

Thermolyses of 2 with TEMPO. **2**, 33 mg (0.061 mmol), was dissolved in 10 mL of benzene; then 0.30 mL of this solution was diluted to 10.0 mL with benzene and 3.25 mL of this solution was placed in a visible cuvette equipped with a side arm. Next, 0.25 mL of 3.20×10^{-2} M TEMPO was added to the side arm. The cuvette was capped and taken

(45) The conductance, L, measured with the conductivity bridge is converted to the molar conductivity, Λ, by the well-known equation $\Lambda = kL/C$, where k is the cell constant and where C is concentration.

out of the box, the TEMPO and **2** were mixed by inverting the cuvette several times just prior to taking the first visible spectrum, and the time was noted; [**2**] = 1.7×10^{-4} M; [TEMPO] = 2.3×10^{-3} M (14 equiv). The contents of the cuvette were thermolysed at 60 ± 0.2 °C, and, again, the reaction was followed periodically by visible spectroscopy. Two more cuvettes were made up in the same fashion and the contents similarly thermolysed at 75 and 90 °C. These reactions were also followed by visible spectroscopy as prescribed above. A BASIC kinetics program written for an IBM PC was used to determine rate constants for these reactions [the program was first verified (shown to give the correct rate constants) using a calculated set of data computed from a known rate constant]. An Eyring plot of rate constants versus temperature was performed to determine activation parameters.

Thermolysis at 69 °C of 2 with TEMPO. The cuvettes from the section below titled **2** + TEMPO Binding Constant Measurement, each with 2.7×10^{-4} M **2** and 1, 2, 10, or 20 equiv of TEMPO, were thermolysed in an oil bath at 69.0 ± 0.1 °C. Four milliliters of the 3.2×10^{-4} M stock solution of **2** from the section below titled "**2** + TEMPO ESR Measurement..." was added to a cuvette with 0.135 mL of the 4.85×10^{-2} M TEMPO stock solution also from the same section below; [**2**] = 3.1×10^{-4} M; [TEMPO] = 1.6×10^{-3} M (5.1 equiv). In the drybox about 10 mg (0.02 mmol) of **1** was dissolved in 15.0 mL of benzene. One milliliter of this solution was diluted to 5.0 mL, transferred to a visible cuvette, sealed, and removed from the box, and the contents were photolysed for about 20 min to form **2**. [**2**] = 2.4×10^{-4} M by visible spectroscopy. The cuvette was returned to the box and 3.5 mL of this solution was transferred to another cuvette. A 0.5-mL sample of a 4.8×10^{-2} M TEMPO solution made by dissolving 26.5 mg (0.170 mmol) in 3.5 mL of benzene was added to the cuvette. [**2**] = 2.1×10^{-4} M; [TEMPO] = 6.1×10^{-3} M (29 equiv). The contents of all cuvettes prepared in this section were thermolysed in a 69.0 ± 0.1 °C oil bath for 26–46 h. The initial time was recorded and the reaction was followed periodically by visible spectroscopy. Rate constants were determined as described above.

Kinetic Studies Done by Numerical Integration. Data from the 69 °C thermolysis of **1** to **1** ⇄ **2**, and **2** to **2** ⇄ **1** (the same data used to plot Figures 4 and 5) were entered into a GEAR/GIT[19] iteration file using Microsoft WORD. Next, using the PRGEAR portion of the program, a GEAR file was made by using the upper portion of Scheme I (equilibrium, in the absence of TEMPO trap). Rate constants were set equal to −1 in this GEAR file so that the GIT program would iterate upon these values ($k_{1,appl}$ and $k_{-1,appl}$) using the experimental data. In fact, both sets of data yielded the same values within experimental error for these rate constants as those determined experimentally, providing considerable confidence in both the raw kinetic data and the resultant rate constants, equilibrium constants, and activation parameters. (See the Results section; modeling plots are found in the supplementary material, Figures B and C.)

2 + TEMPO **Binding Constant Measurement.** In the drybox approximately 11 mg (0.020 mmol) of **1** was dissolved in 15.0 mL of benzene and photolysed for about 20 min to form **2**. Four milliliters were transferred to a visible cuvette, removed from the box, and analyzed by visible spectroscopy; [**2**] = 1.35×10^{-3} M. TEMPO, 21.2 mg (0.136 mmol), was dissolved in 10.0 mL of benzene; [TEMPO] = 1.36×10^{-2} M. Solutions of 2.7×10^{-4} M **2** and 0, 1, 2, 10, and 20 equiv of TEMPO were made by mixing the appropriate volumes of the two stock solutions and diluting to 5.0 mL. Samples were transferred to visible cuvettes, removed from the box, and analyzed by visible spectroscopy. All handling of these samples was done in the dark at ambient temperature to prevent reaction of **2** with TEMPO. There was no change in the visible spectrum of **2** as a function of equivalents of TEMPO [outside of dilution (3%)] in these experiments. Hence we conclude that TEMPO does not coordinate to the vacant coordination site on **2**.

2 + TEMPO **ESR Measurement Probing for a 2·TEMPO Adduct.** It was conceivable, albeit perhaps unlikely, that the observed zero order in TEMPO kinetics could have been explained by the 100% formation of a 2·TEMPO adduct; hence this was probed for by the following ESR experiment. In the drybox approximately 2 mg (0.004 mmol) of **1** was dissolved in 15.0 mL of benzene. Four milliliters was transferred to a visible cuvette, removed from the box, photolysed for about 20 min to form **2**, and analyzed by visible spectroscopy; [**2**] = 3.2×10^{-4} M. TEMPO, 75.8 mg (0.485 mmol), was dissolved in 10.0 mL of benzene; [TEMPO] = 4.85×10^{-2} M. The TEMPO stock solution, 0.33 mL, was diluted to 5.0 mL with benzene, [TEMPO] = 3.2×10^{-4} M. A 0.5-mL sample of this TEMPO solution was added to an airtight NMR tube containing 0.5 mL of benzene. The tube was sealed, removed from the box, and analyzed by ESR. After analysis, the tube was cleaned thoroughly and returned to the box. The 3.2×10^{-4} M solution of **2**, 0.5 mL, was added to the same airtight NMR tube containing 0.5 mL of benzene. The tube was sealed, removed from the box, and analyzed by ESR. After analysis, the tube was again cleaned thoroughly and returned to the box. Finally, 0.5 mL of the 3.2×10^{-4} M solution of **2** and 0.5 mL of the 3.2×10^{-4} M solution of TEMPO were added to the same airtight NMR tube. Again, the tube was sealed, removed from the box, and analyzed by ESR. The X-band ESR spectrum of TEMPO by itself was clearly visible. There was no detectable ESR spectrum of **2** by itself. When equivalent amounts of **2** and TEMPO were mixed, the three-band spectrum of TEMPO was still visible. The areas of the two spectra (TEMPO and TEMPO + **2**) were equivalent as well. If TEMPO were coordinating to **2**, its ESR spectrum should be changed, but it was not. Hence, there is no ESR-detectable **2**·TEMPO adduct and this conceivable explanation of the zero-order TEMPO kinetics is ruled out.

Acknowledgment. Support from NIH Grant DK 22614, and especially the support of this undergraduate research project,[1] as one component of that grant, is gratefully acknowledged.

Supplementary Material Available: Figure A, showing Newman projections of two possible solution diastereomers of **2** that were considered as a possible explanation for the presence of the two downfield proton peaks in the ^{1}H NMR of **2**; Figures B and C, showing respectively the curve fit from the GEAR/GIT modeling of the thermolysis of **1** or **2** to the equilibrium mixture, **1** ⇄ **2**; Figures D and E, showing GEAR-generated concentration versus time plots, using experimentally determined rate constants, of the thermolysis of **1** (or **2**) with TEMPO trap to show the potential formation of **2** (or **1**) during the reactions; Figure F, showing the bimolecular Kochi/Espenson-type mechanism[30] that was considered but ruled out on the basis of the observed first-order kinetics; derivation of the kinetics equations for $k_{1,TEMPO}$, $k_{2,TEMPO}$, $k_{1,appl}$, and $k_{-1,appl}$ in terms of the rate constants for elementary steps shown in Scheme III (13 pages). Ordering information is given on any current masthead page.